SIAM REVIEW
Vol. 48, No. 4, pp. 629–678

Mode-Locked Soliton Lasers*

J. Nathan Kutz†

Abstract. A comprehensive treatment is given for the formation of mode-locked soliton pulses in optical fiber and solid state lasers. The pulse dynamics is dominated by the interaction of the cubic Kerr nonlinearity and chromatic dispersion with an intensity-dependent perturbation provided by the mode-locking element in the laser cavity. The intensity-dependent perturbation preferentially attenuates low intensity electromagnetic radiation which makes the mode-locked pulses attractors of the laser cavity. A review of the broad spectrum of mode-locked laser models, both qualitative and quantitative, is considered with the basic pulse formation phenomena highlighted. The strengths and weaknesses of each model are considered with two key instabilities studied in detail: Q-switching and harmonic mode-locking. Although the numerous mode-locking models are considerably different, they are unified by the fact that stable solitons are exhibited in each case due to the intensity discrimination perturbation in the laser cavity.

Key words. optical fibers, solitons, mode-locking, stability, lasers

AMS subject classifications. 35Q55, 35B32, 35B20, 78A60, 41A60

DOI. 10.1137/S0036144504446357

1. Introduction.

The invention of the laser in 1960 is a historical landmark of scientific innovation [1]. In the four-and-a-half decades since, the laser has evolved from a fundamental science phenomenon to a ubiquitous, cheap, and readily available commercial commodity. A large variety of laser technologies and applications exists from the commercial, industrial, medical, and academic arenas [2]. In optical communications, for instance, the laser is a compact, reliable, and cheap lightwave source at the wavelength of 1.55 microns for applications in high-speed fiber-optic communications systems and interconnection networks. For this application, the laser is required to produce ultrashort pulses (e.g., 200 femtoseconds–50 picoseconds pulse widths), which are in fact solitons [3], with nearly uniform amplitudes. The generation of such soliton pulses is the subject of this survey article and is often referred to as *mode-locking* [4, 5].

In an optical fiber laser cavity, the underlying wave behavior is governed by the the nonlinear Schrödinger equation (NLS). The NLS is derived from a high-frequency asymptotic expansion of Maxwell's equations by using the paraxial approximation, rotating-phase approximation, and quasi-monochromatic wave assumption in succession [6, 7]. The dominant physical effects are then the chromatic dispersion and a weak Kerr nonlinearity [8]:

$$i\frac{\partial Q}{\partial Z} + \frac{1}{2}\frac{\partial^2 Q}{\partial T^2} + |Q|^2 Q = 0\,. \tag{1}$$

*Received by the editors October 19, 2004; accepted for publication (in revised form) October 5, 2005; published electronically November 2, 2006. This work was supported by NSF grant DMS-0092682.

http://www.siam.org/journals/sirev/48-4/44635.html

†Department of Applied Mathematics, University of Washington, Box 352420, Seattle, WA 98195-2420 (kutz@amath.washington.edu).

Here Q is the electric field envelope, Z represents the propagation distance in the fiber, and T is the time in the rest frame of a moving pulse [6, 7]. The NLS has been investigated extensively in this context with particular emphasis given to the robust and stable soliton solutions of the hyperbolic secant form,

$$Q(Z,T) = \operatorname{sech} T \exp(iZ/2)\,, \tag{2}$$

which result from a fundamental balance between the linear dispersion and the cubic nonlinearity. Although many other effects are present in the fiber, such as linear attenuation, third-order dispersion, polarization dynamics, higher-order nonlinear effects, or saturable absorption, it is the combined effects of the cubic nonlinearity and temporal dispersion which eventually dominate the stability and behavior of the resulting soliton pulse train.

It should be noted that in what follows the term soliton is used in a much broader sense than the strict mathematical definition of a solution of a completely integrable nonlinear partial differential equation [9]. Rather, the optics community refers to any localized structure which is robust and persists under a large class of perturbations as a soliton. This includes stable localized solutions of dissipative systems (*dissipative solitons*) which are clearly not integrable or Hamiltonian [10].

From a physical standpoint, the successful operation of a mode-locked laser is achieved by utilizing so-called *additive-pulse mode-locking* (APM) [11, 12] or *Kerr-lens mode-locking* (KLM) [13, 14] action, which is simply an *intensity discrimination* perturbation in the laser cavity, in conjunction with bandwidth limited gain. In its simplest form, an APM/KLM (intensity discrimination) component within the laser cavity preferentially attenuates weaker intensity portions of individual pulses. This attenuation is compensated for by the gain medium (e.g., erbium-doped fiber), which acts to preserve the total cavity energy. Thus pulse shaping occurs since the peak of a pulse experiences a higher net gain per round trip than its lower intensity wings. This time-domain narrowing (compression) of a propagating pulse is limited, however, by the bandwidth of the gain medium (typically $\approx 20 - 40$ nm [4, 5]). This mode-locking mechanism, which is only a small perturbation to the NLS (1), has been successfully achieved in a wide variety of experimental configurations, including a fiber ring laser with a linear polarizer [15, 16, 17, 18], the figure-eight laser with nonlinear interferometry [19, 20, 21, 22], a linear-cavity configuration with a semiconductor saturable absorber [23, 24, 25], and a cavity with an acousto-optic modulator [26, 27].

To help illustrate how intensity discrimination is achieved, we consider a variety of physically realizable laser cavity configurations. Note that the remainder of the article will serve to supplement this cursory, qualitative description. For the ring laser in Figure 1(a), the Kerr nonlinearity of the birefringent optical fiber generates a nonlinear rotation of the polarization state that depends on the pulse intensity. The insertion of a passive polarizer provides an effective intensity filter which mode-locks a propagating pulse by periodically attenuating all components of the pulse which are not aligned with the polarizer [15, 16, 17, 18]. Thus only pulse intensities with the correct nonlinear polarization rotation are preserved. In a similar fashion, the inclusion of a saturable Bragg reflector (SBR) in the linear cavity configuration of Figure 1(b) leads to stable pulse formation. The SBR acts to preferentially attenuate low intensity portions of a pulse, whereas high intensity portions of a pulse are minimally attenuated since they quickly saturate the SBR and pass through without loss [23, 24, 25]. Nonlinear mode-coupling is the basis of several proposed mode-locking models [28] and is illustrated in Figure 1(c) with a long-period fiber grating

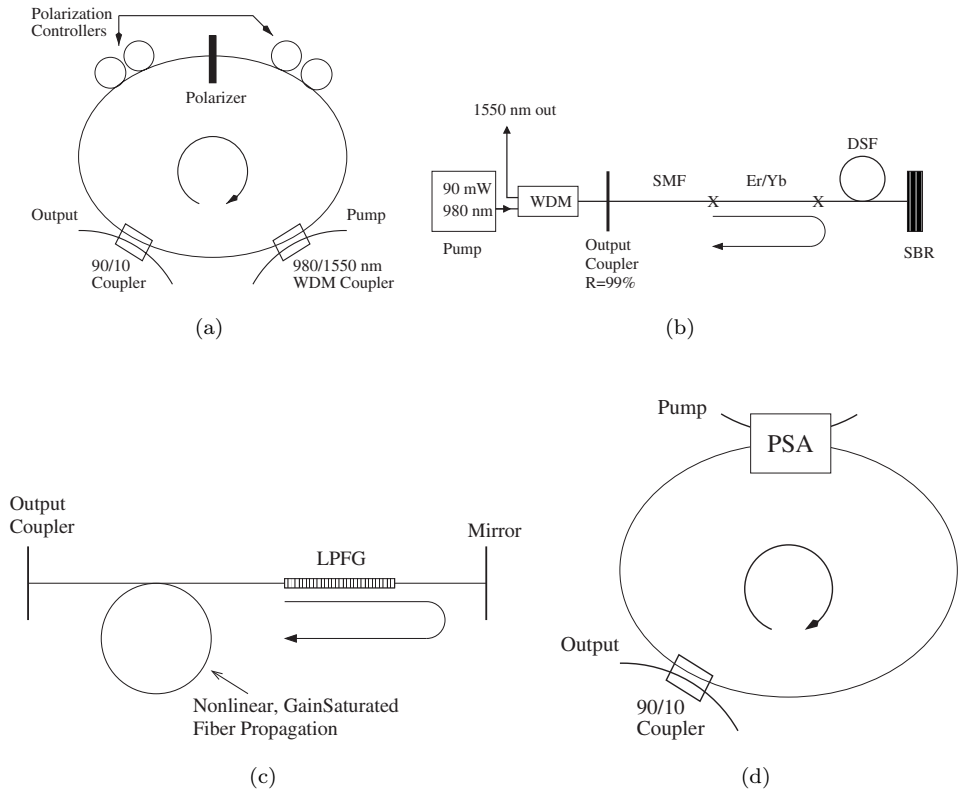

Fig. 1 *Some typical fiber cavity configurations.* (a) *Schematic of the ring cavity laser that includes a passive polarizer and polarization controllers in a birefringent optical fiber* [15, 16, 17, 18]. *A small portion of the fiber is actually erbium-doped fiber which is pumped via a wavelength-division multiplexed (WDM) coupler at* 980 *nm and provides gain to the cavity. The mode-locked soliton pulse stream is coupled out through a* 90/10 *coupler, i.e.,* 10% *of the light is coupled out.* (b) *A linear cavity configuration which includes an SBR, single mode fiber (SMF), dispersion shifted fiber (DCF), erbium/ytterbium gain fiber (Er/Yb), and a* 99/1 *output coupler* [23, 24, 25]. (c) *A proposed linear cavity configuration with an LPFG which induces nonlinear mode-coupling to the fiber cladding modes.* (d) *A proposed ring cavity which uses phase-sensitive amplification to overcome attenuation. The phase-sensitive amplifier preferentially amplifies pulses which are aligned in phase with the amplifier.*

(LPFG). For this case, low intensity portions of a pulse are resonantly coupled to a fiber cladding mode and attenuated. High intensities, however, are detuned from resonance and pass through the grating with only minimal attenuation. Thus intensity discrimination is achieved with nonlinear mode-coupling [28]. Finally, Figure 1(d) achieves intensity discrimination through nonlinear phase rotation. In this case, the mode-locking element is a phase-sensitive amplifier which amplifies only phase components which are aligned with the amplifier. Only pulses which achieve a nonlinear phase rotation commensurate with the amplifier are preserved. In all cases, the intensity discrimination is a small perturbation to the NLS (1) which acts to make the one-soliton solution an *attractor* of the laser cavity system.

Mode-locking, then, results from the interplay of the NLS one-soliton dynamics with a small, intensity-dependent perturbation. The time scale of the perturbation

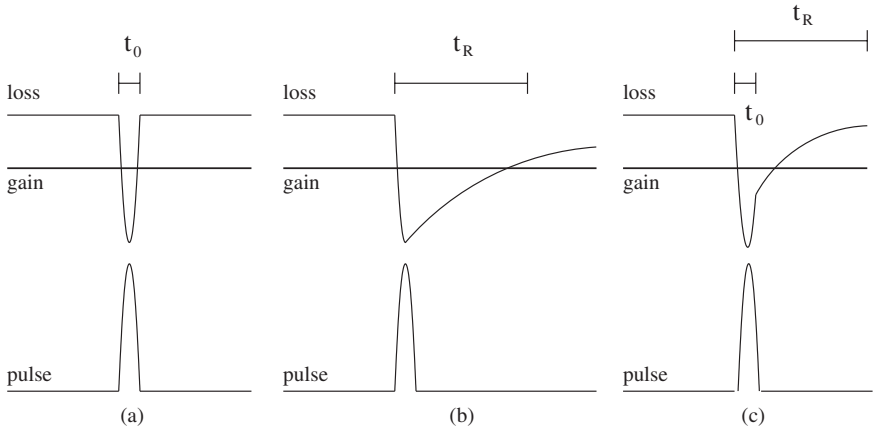

Fig. 2 *Qualitative depiction of the mode-locking mechanism. The mode-locking element results in an intensity discrimination which gives a small window of net gain in the cavity around the mode-locked pulse. The net gain can be an instantaneous response which occurs on the time scale t_0 of the pulse width (depicted at left). Alternatively, it can be an instantaneous response followed by a slow recovery on a time scale t_R which is much longer than t_0 (middle figure). Or in certain cases, the mode-locking element can have both an instantaneous and a slow response (depicted at right). In all three cases, a gain window is created for the pulse which gives rise to the necessary pulse shaping mechanism required for mode-locking.*

is itself of importance. Specifically, the intensity discrimination typically falls into three different categories: an instantaneous response, a slow response, and a mixed (fast and slow) response. Figure 2 shows the three cases in turn. In Figure 2(a), the fast response acts instantaneously across the pulse to create a window of net gain by lowering the attenuation around the peak of the pulse. This gives the intensity discrimination necessary to achieve mode-locking. In Figure 2(b), a slow response is shown which can arise when using saturable absorbers. In this case, the leading edge of the pulse is absorbed and the peak of the pulse then experiences a lower attenuation. However, the recovery time of the absorber allows for a net gain window which can extend far beyond the pulse. Regardless, the gain window is sufficient to begin the mode-locking process. Finally, in Figure 2(c), certain lasers are mode-locked by a combination of both fast (instantaneous) and slow recovery time processes. This occurs, for instance, when mode-locking with a saturable absorber just below the exciton peak [24, 25]. Again, a net gain window is created which allows for the formation of mode-locked pulses.

A natural conclusion from the preceding exposition is that prior to soliton formation, more general models than the NLS (1) are required to determine the pulse formation and soliton stabilization dynamics. The canonical model, which qualitatively describes both the energy saturation and the pulse stabilization process in a solid-state laser, is the *master mode-locking equation* [11, 12]. The master mode-locking model is a perturbation from the NLS model which was proposed to capture two key effects: the equilibration of the pulse energy, and the consequent balance of nonlinearity and dispersion in forming stable pulses. Because it achieves both these goals, the master mode-locking equation is widely considered to be the most successful model developed for a phenomenological description of mode-locking. The dominant contributions from chromatic dispersion and the cubic Kerr nonlinearity can also be

shown to lead to mode-locked pulse formation using methods of statistical mechanics [29, 30, 31]. This statistical analysis is an effective way to capture the start-up dynamics in the laser cavity.

However, the master mode-locking description is limited to systems where spatial [32] and higher-order [33] dispersion effects are negligible. Further, it does not include polarization dynamics, active modulation, mode-coupling, or a quantitatively meaningful saturable absorption component. It is, by construction, a qualitative model. Additionally, only a small range of parameters allow for the formation of stable mode-locked soliton pulses. To overcome this limitation, various phenomenological terms, such as hyperdiffusion and quintic nonlinear absorption, can be used to augment the master mode-locking model. This broadens the scope of possible solutions as well as the parameter space for which these solutions can be observed. Regardless, the models remain qualitative in nature and no direct quantitative agreement has been achieved with experiment. The first part of this article reviews the various qualitative models used to characterize the phenomenon of soliton mode-locking.

Quantitative modeling of mode-locked laser cavities requires improved model descriptions which account for the additional physical effects allowing for the mode-locking to occur. Thus each type of mode-locked laser must be modeled independently. These models are also perturbations from the NLS equation and rely on the underlying hyperbolic-secant pulse solutions of the NLS which represent the ideal mode-locked pulses. However, the models can vary drastically from one another as they account for significantly different mechanisms for intensity discrimination in the laser cavity. In the second part of this work, a wide variety of mode-locking models are considered which capture physical phenomena beyond the scope of the master mode-locking description. The fundamental aim of these models is to provide a quantitative analysis of a laser cavity and make direct connection with and verification of physically realizable mode-locked lasers. Further, in the context of quantitative modeling, the stable operating regimes of a given laser can be mapped out in parameter space.

This manuscript gives an overview and comprehensive treatment of the mode-locking models used to study the pulse dynamics in laser cavities. The primary focus is on capturing both the mode-locking development and the resulting pulse train dynamics which are dominated by the cubic nonlinearity and dispersion. These are heavily influenced by various perturbations in the fiber such as the passive polarizer, saturable absorber, mode-coupling, or active modulation element. In section 2 of the paper, a review is given of the qualitative models used to describe mode-locking. Section 3 considers the quantitative models which have been developed to describe existing mode-locking technologies. The discussion of quantitative models is extended in section 4 which considers theoretical mode-locking configurations and models which have yet to be experimentally realized. A review of each model is given with an evaluation of its strengths and weaknesses. Although the models are different, they are unified by the fact that stable, solitary waves, i.e., solitons, are exhibited in each case. Section 5 presents a discussion of instabilities and additional effects which are commonly observed in mode-locked cavities. Some of these effects are beneficial and others pernicious depending upon the desired application. A summary with the key aspects and common features of the mode-locking models is given in the final section.

2. Qualitative Mode-Locking Models. Characterizing the mode-locked solitons in optical fiber lasers is the balance between the nonlinearity and dispersion given by the NLS (1). Achieving the soliton state, however, requires a form of intensity discrimination. In the following subsections, a variety of models are explored which

incorporate different phenomenological terms which lead to the stable development of mode-locked pulse trains. We begin with the master mode-locking model [11, 12], which is the generic and canonical description, and move into more complicated models which have various advantages over the basic master mode-locking description.

2.1. Master Mode-Locking. The key element in deriving the master mode-locking model is a physical system which exhibits nonlinearity, dispersion, bandwidth limited gain, energy saturation, and APM action (intensity discrimination). All these elements are crucial for self-starting and stabilization of a constant-energy pulse. These effects can be combined to generate the master mode-locking model [11, 12]

$$i\frac{\partial Q}{\partial Z} + (1 - i\tau g(Z))\frac{\partial^2 Q}{\partial T^2} + (4 - i\beta)|Q|^2 Q + i(\gamma - g(Z))Q = 0, \tag{3}$$

where

$$g(Z) = \frac{2g_0}{1 + \|Q\|^2/e_0} \tag{4}$$

and Q represents the electric field envelope normalized by the peak field power $|Q_0|^2$. Here the variable T represents the physical time in the rest frame of the pulse normalized by $T_0/1.76$, where T_0 is the full width at half maximum (FWHM) of the pulse (e.g., $T_0 = 200$ fs). The variable Z is scaled on twice the dispersion length $Z_0 = (4\pi c)/(\lambda_0^2 \bar{D})(T_0/1.76)^2$ corresponding to the average dispersion. This then gives the peak field power $|Q_0|^2 = 2\lambda_0 A_{\text{eff}}/(\pi n_2 Z_0)$. Note that $\|Q\|^2 = \int_{-\infty}^{\infty} |Q|^2 dT$. Further, for all models discussed $n_2 = 2.6\times 10^{-16}$ cm^2/W is the nonlinear coefficient in the fiber, $A_{\text{eff}} = 60$ μm^2 is the effective cross-sectional area of the fiber, $\Gamma = 0.2$ dB/km is the fiber loss, and $\lambda_0 = 1.55$ μm and c are the free-space wavelength and speed of light, respectively.

The remaining parameters can vary largely from experiment to experiment. In terms of the scaling variables, we have $e_0 = E_0/|Q_0|^2$, $g_0 = G_0 Z_0$, $\gamma = \Gamma Z_0$, $\beta = B|Q_0|^2 Z_0$, and $\tau = (1/\Omega^2)(1.76/T_0)^2$. Here B (in 1/Watt/meter) is the parameter that controls the strength of the phenomenological model of the nonlinear saturable absorption and G_0 (in 1/meter) is the linear gain from amplification. For a gain bandwidth which can vary from $\Delta\lambda = 20 - 40$ nm, we find that $\Omega = (2\pi c/\lambda_0^2)\Delta\lambda$ so that τ varies from $\approx 0.08 - 0.32$ for a pulse width of $T_0 = 200$ fs. Note that τ is the parameter which largely controls the resulting pulse width of the stabilized mode-locked pulse stream since it limits the spectral gain bandwidth of the mode-locking process.

We consider mode-locked pulse solutions to the master mode-locking model (3). Chirped soliton solutions to (3) are constructed in the form [34]

$$Q(Z,T) = \eta\,\text{sech}(\omega T)^{1+iA}\exp(i\theta Z), \tag{5}$$

where η, ω, A, and θ are real constants. These explicit solutions, however, exist only if the energy of the mode-locked pulses is at the saturation level e_0 so that $e_0 = \|Q\|^2$. Here we assume that the constants g_0, γ, and β are small so that (3) can be considered using perturbation techniques [35, 36, 37]. The primary effect of the perturbation on the soliton is an additional phase chirp A. If all constants aside from β are fixed such that $\gamma < 2g_0$, then the following is found [36, 37]: For $\beta \le 0$, there is a unique soliton. For $0 < \beta < \beta_*$, there are precisely two solitons, both of which are unstable. For $\beta_* < \beta < \beta^*$, there are precisely two solitons, one of which is stable. Last, for

$\beta > \beta^*$, there are no solitons since the nonlinear gain is too large to sustain a pulse with finite energy. The behavior of the solutions (5) of (3) for these different values of β is considered below. Stable mode-locked solutions are found only for $\beta \in (\beta_*, \beta^*)$ as shown by the bifurcation structure of the solution (5) in [37].

The mode-locking stability and dynamics are explored with numerical simulations of the governing equation (3). The numerical procedure employed for this model and all others considered here uses a fourth-order Runge–Kutta method in Z and a filtered pseudospectral method in T. In the calculations and simulations that follow, we scale all parameters on the FWHM pulse width $T_0 = 200$ fs and assume that the master mode-locking parameters are $e_0 = 1.0, g_0 = 0.1, \tau = 0.1$, and $\gamma = 0.1$. The remaining free parameter β is the bifurcation parameter which determines the stability of the pulse solutions. These values give $\beta_* = 0.01$ (radiation-mode instability) and $\beta^* = 0.0348$ (saddle-node instability) [36, 37]. Thus, there are four distinct regions of behavior.

To illustrate the possible mode-locking behaviors, we first consider the stable regime for which $\beta_* = 0.01 < \beta < 0.0348 = \beta^*$. Figure 3(a) depicts the evolution to a steady-state pulse solution given an arbitrary initial condition and $\beta = 0.034$. Over approximately 400 units, the pulse readjusts its height, width, and energy to reach an equilibrium pulse solution. This stable evolution is the ideal behavior of the master mode-locking model. The instabilities are also easily captured computationally. For $\beta = -0.05 < 0$, the unstable radiation modes together with nonlinear damping lead to the instability illustrated in Figure 3(b) [36, 37]. In this case, the initial localized pulse energy is quickly transferred into quasi-periodic behavior. So although the pulse energy is kept in control by the gain model, the pulse continues to oscillate as depicted by the continued fluctuations in Figure 3(b). The oscillatory dynamics persists as $Z \to \infty$. This behavior is characteristic of simulations with $\beta < 0$. For $0 < \beta < 0.01 = \beta_*$, the pulse is destabilized by radiation modes [36, 37]. Since the radiation modes are, strictly speaking, present only in the infinite domain, the computational method with periodic boundary conditions gives rise to the instability depicted in Figure 3(c). In this case, the amplitude continues to fluctuate and a steady state is never achieved. The energy which accumulates at the boundary is a manifestation of a finite computational domain. Regardless, the pulse destabilizes and although the cavity energy reaches equilibrium, oscillations persist as $Z \to \infty$. Finally, for values of $\beta > 0.0348 = \beta^*$, the nonlinear gain is too high to be overcome by the linear loss mechanisms present in the master mode-locking equations [36]. The solution quickly grows and blow-up occurs. The onset of blow-up is shown in Figure 3(d) for $\beta = 0.035$. Note that by $Z = 52$, the pulse intensity has grown fivefold. Just after $Z = 56$, the pulse solution undergoes self-similar collapse, and it is no longer computationally feasible to resolve the evolution. Thus the three regions of unstable behavior are markedly different (see Figures 3(b)–(d)) and present limitations to the use of the master mode-locking model.

Since the master mode-locking equation is the canonical model describing both the energy saturation and the pulse stabilization process in a solid-state laser, regions of stable operation can be predicted within an analytic framework [36, 37]. Further, general trends in the expected mode-locking can be understood as a function of key physical parameters such as the gain bandwidth and cavity dispersion. The successful operation of the laser is achieved by having a sufficient amount of saturable absorption. Otherwise, the laser is subject to a radiation-mode instability. Likewise, if the nonlinear gain is too high, the linear attenuation terms are unable to prevent the pulse from blowing up, suggesting the breakdown of the master mode-locking model. Although

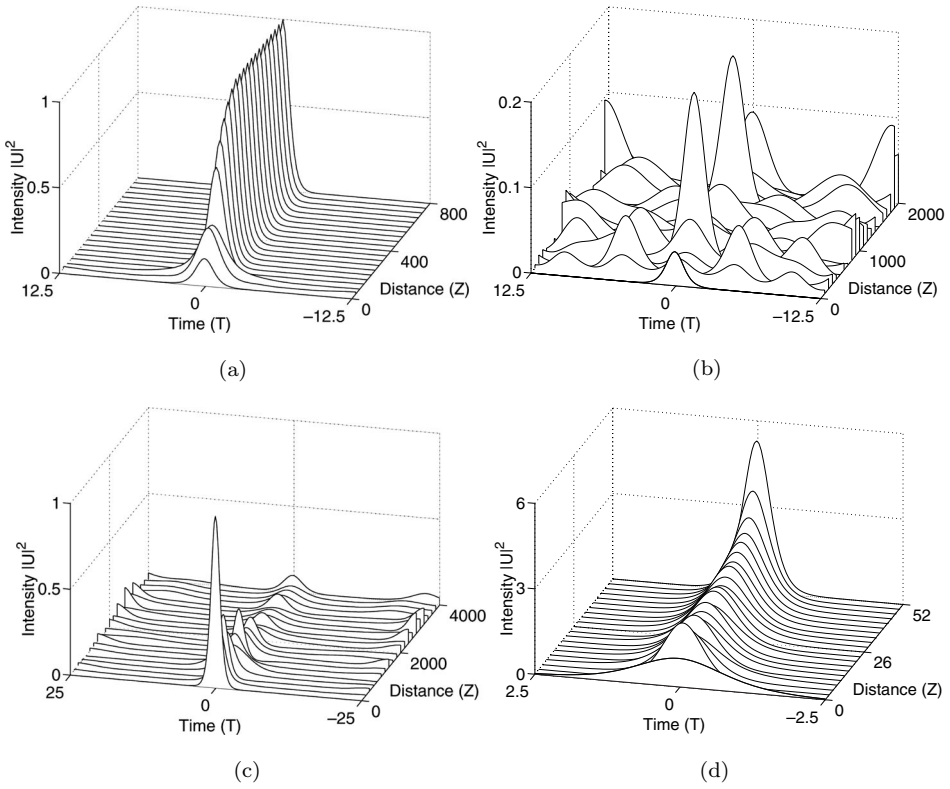

Fig. 3 *Mode-locking dynamics in the master mode-locking model.* (a) *Stable mode-locking evolution for* $\beta = 0.034$ *which quickly settles to the steady-state pulse solution.* (b) *Unstable evolution for* $\beta = -0.05$ *which quickly evolves into a nonlocalized weak-turbulence regime which persists over time.* (c) *Unstable evolution for* $\beta = 0.005$ *which quickly evolves into a nonlocalized quasi-periodic solution. Although the cavity energy is controlled by the time-dependent gain of the master mode-locking equation, the quasi-periodic oscillations persist.* (d) *Unstable evolution for* $\beta = 0.035$ *where the pulse quickly blows up. In this case, the cavity energy is not controlled by the time-dependent gain of the master mode-locking equation.*

it is a valuable tool for analysis, the master mode-locking model fails to capture many physically relevant behaviors exhibited in practical mode-locked systems.

2.2. Extending Master Mode-Locking: Cubic-Quintic Models. The master mode-locking model proposed by Haus is elegant and efficient in capturing the key qualitative aspects of the intensity discrimination and propagation in a laser cavity. However, it suffers drawbacks on two accounts. First, it is not a quantitative model, which makes it difficult to compare with and make predictions concerning experimental systems. Second, there is only a small window of parameter space which allows for the generation of stable mode-locked pulses. In particular, the model is highly sensitive to the nonlinear loss/gain parameter β. For the physically reasonable values of parameters considered in the last section, it is required that $0.01 \leq \beta \leq 0.0348$. Otherwise, the solution may blow up or undergo a radiation-mode instability [36].

The sensitivity to the parameter β can be easily overcome by augmenting the master mode-locking equation with a quintic saturation term. This prevents the blow-

up of solutions and allows for a drastically larger range of values for the parameter β. The addition of a saturating quintic term is a standard method for regularizing Ginzburg–Landau-type equations [38], including the master mode-locking model [39, 40, 41, 42, 43]. Recall that the cubic gain of the master mode-locking equation is purely phenomenological. The addition of the quintic term provides a saturation to the nonlinear growth which is expected in any physically realizable system. The quintic master mode-locking equation is then

$$i\frac{\partial Q}{\partial Z} + (1 - i\tau g(Z))\frac{\partial^2 Q}{\partial T^2} + (4 - i\beta)|Q|^2 Q + i\sigma|Q|^4 Q + i(\gamma - g(Z))Q = 0, \tag{6}$$

where the parameter $\sigma \ll 1$ provides a small amount of quintic saturation which prevents blow-up of solutions to the standard master mode-locking equation. The addition of the quintic term no longer allows for the construction of exact solutions to (6). Thus, from an analytic framework, the quintic term can be treated as a perturbation to the solutions of the cubic master mode-locking [38].

For the standard master mode-locking equation (3), solutions are unstable for a fixed gain parameter $g(Z) = g_0$ [38]. Thus a saturated gain model is introduced in (4) which allows for stable solutions [36, 37]. In contrast, the quintic master mode-locking model (6) does not require a saturated gain model since a constant gain can also stabilize solutions. Thus there are two standard models for the gain dynamics of the quintic master mode-locking:

$$\text{model 1:} \qquad g(Z) = \frac{2g_0}{1 + \|Q\|^2/e_0}, \tag{7a}$$

$$\text{model 2:} \qquad g(Z) = g_0\,. \tag{7b}$$

In the first model, the standard saturated gain model of master mode-locking is carried over to the quintic case. The second model simply fixes the gain to be a constant g_0 which is sufficiently large to overcome the linear losses in the cavity. The quintic saturation then provides a nonlinear attenuation of the solution once the cavity energy becomes sufficiently large. Since the quintic master mode-locking is qualitative in nature, either model given by (7) is an acceptable description of the gain dynamics.

Figure 4 illustrates the dynamics of the quintic master mode-locking equation with both the saturating gain and constant gain models. Specifically, the parameter β is chosen to be $\beta = 0.1 > \beta^*$ in the simulations so that we are well beyond the stability criteria ($\beta^* = 0.0348$) of the standard master mode-locking model. Panel (a) demonstrates the solution blow-up which occurs for the standard mode-locking model (6) with $\sigma = 0$. For $\sigma = 0.02 > 0$, saturation occurs and the dynamics settles to a mode-locked pulse solution. Panel (b) demonstrates the dynamics for the saturated gain model (7a). For this simulation $g_0 = 0.1$ with $e_0 = 1, \tau = 0.1$, and $\gamma = 0.1$. Using the same basic parameters, panel (c) shows similar results to panel (b) with a fixed gain of $g_0 = 0.05$ in (7b). The parameter g_0 is chosen to give approximately the same saturating L^2 norm as for the saturated gain model. The L^2 norm dynamics is demonstrated for all three simulations in the lower right panel of Figure 4. Note that the quintic term has the desired effect of greatly extending the stability range in parameter space of the mode-locked pulse solution.

2.3. Mode-Locking with Saturable Absorbers. Both the cubic and quintic master mode-locking models of the previous two sections account for the mode-locking element in an instantaneous fashion through the cubic or quintic attenuation terms.

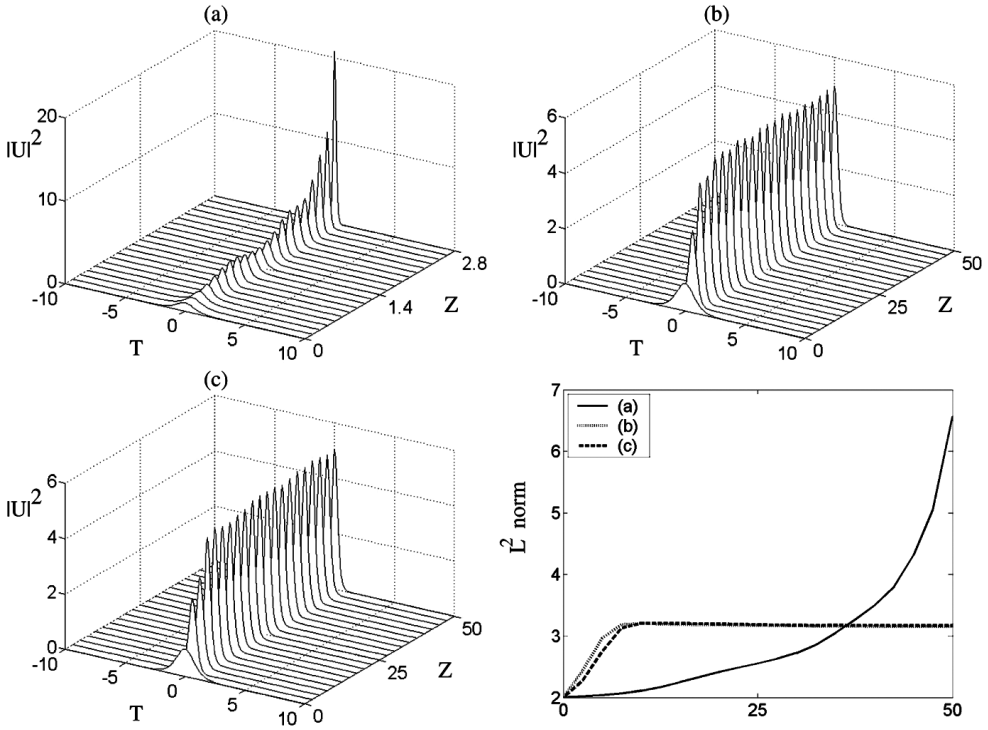

Fig. 4 *Quintic master mode-locking dynamics for the parameter* $\beta = 0.1$ *with* $\tau = 0.1, \gamma = 0.1$, *and* $e_0 = 1$. *Panel* (a) *demonstrates the typical master mode-locking blow-up which occurs with* $\sigma = 0$. *With quintic saturation added* ($\sigma = 0.02$), *the dynamics settles to a mode-locked pulse solution for the saturated gain model* (7a) *(panel* (a) *with* $g_0 = 0.1$*) and the constant gain model* (7b) *(panel* (b) *with* $g_0 = 0.05$*). In the lower right, the saturation of the* L^2 *norm is illustrated for these three cases.*

However, many mode-locking processes are not instantaneous (see Figure 2). As a specific example, mode-locking with a saturable absorber requires modification of the governing master mode-locking equation to capture the time dependence of the saturation and recovery processes. Including the saturable absorber dynamics in the master mode-locking equation gives [23, 27]

$$i\frac{\partial Q}{\partial Z} + (1 - i\tau g)\frac{\partial^2 Q}{\partial T^2} + 4|Q|^2 Q + i(n(Z,T) + \gamma - g)Q = 0, \tag{8}$$

where now the nonlinear pulse shaping and attenuation occur through the parameter $n(Z,T)$, which evolves according to the absorption model

$$\frac{dn}{dT} = -\frac{n - n_0}{T_d} - \frac{|Q|^2}{e_A}\,. \tag{9}$$

In this model, the parameter T_d is the recovery time of the absorber normalized by the pulse width and e_A is the saturation energy of the absorber normalized by the one-soliton pulse energy of (8) with $\gamma = g = n = 0$. The dynamical equation for $n(Z,T)$ is a first-order differential equation in T which has the solution

$$n(Z,T) = \exp(-T/T_d)\int_{-\infty}^{T} \exp(\xi/T_d)\left(\frac{n_0}{T_d} - \frac{|Q(Z,\xi)|^2}{e_A}\right) d\xi\,. \tag{10}$$

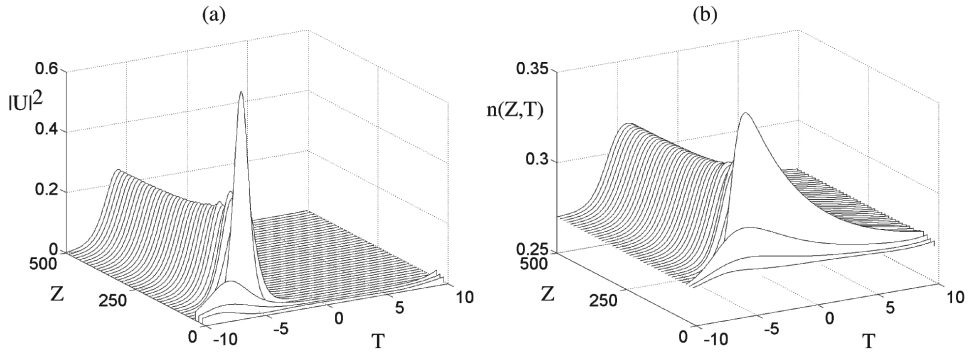

Fig. 5 *Stable mode-locking with a slow-saturable absorber. The parameters to achieve this are* $\tau = 0.1$, $\gamma = 0.6$, $e_A = 10$, $n_0 = 0$, $g = 0.87$, *and* $T_d = 5$. *The pulse intensity is illustrated in* (a) *while the saturation* $n(Z,T)$ *of the absorber is presented in* (b). *Note the formation of the pulse on the left-hand side of the computational domain which results from boundary effects due to the finite computational interval of integration of* (10), *i.e., over the computational domain chosen* $n(Z,T)$ *has not completely decayed to zero. Thus the cavity gain, given by* $n(Z,T)$ *in* (b), *is maximized by the pulse formation at the left edge of the computational domain.*

This expression can be inserted into (8) to give a more complicated nonlocal, nonlinear term in the partial differential equation (3) for the mode-locking dynamics.

This model characterizes the saturation and recovery responses in the laser cavity and brings two key parameters into the mode-locking dynamics: T_d and e_A. The normalized recovery time is of greatest interest since the absorber typically recovers on a time scale much longer than the pulse width. Thus the instantaneous aspects of the mode-locking element are removed. Regardless, this slow response in conjunction with standard soliton formation dynamics can be used as the basis of a mode-locked laser. Kärtner and Keller [23] showed that even for values up to $T_d = 20$, mode-locking can be effectively achieved with ultrashort pulses. This would give a recovery time on the order of several picoseconds for the saturable absorber, which is certainly within physically realizable limits. Experimental evidence has confirmed this ultrashort pulse mode-locking using a slow saturable absorber [44].

Although the model proposes a greatly improved and more realistic description of the saturable absorber dynamics, it is very difficult to computationally stabilize solutions to (8) with (9), i.e., the basin of attraction for the mode-locked pulse solutions is very small in parameter space. In particular, the strong sensitivity to the parameters T_d, e_A, and especially g is significant with solutions mostly decaying to zero or demonstrating blow-up. This fact adversely affects the usefulness of this mode-locking model. If direct quantitative comparison could be made with experiment, then this drawback could perhaps be overlooked. However, no such direct quantitative comparison has been made and the model remains qualitative in nature and much less useful than, for instance, the quintic master mode-locking model which is robust and allows for the generation of mode-locked pulse solutions for a wide range of parameter space. Regardless, it is the only model developed to date which explicitly accounts for mode-locking formation exclusively with a slow, intensity-dependent saturation response.

Figure 5 illustrates the dynamics of the saturable absorber master mode-locking equation (8) along with the saturable absorber dynamics (9). For the simulations, we

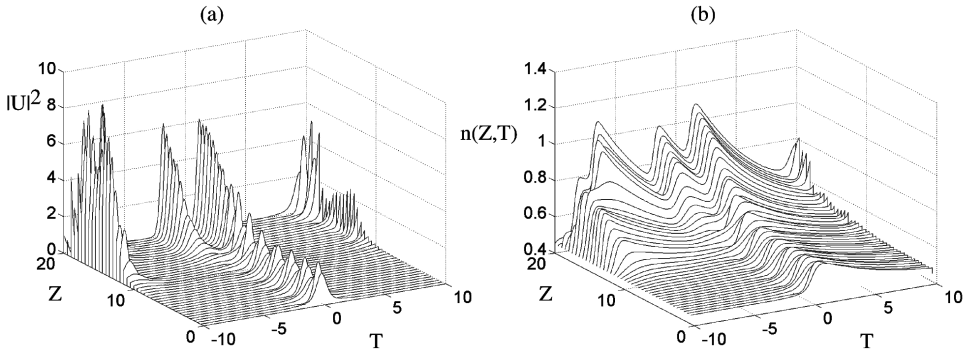

Fig. 6 *Multipulse mode-locking formation with a slow-saturable absorber. The parameters to achieve this are* $\tau = 0.1$, $\gamma = 0.6$, $e_A = 10$, $n_0 = 0$, $g = 1.05$, *and* $T_d = 5$. *The pulse intensity is illustrated in* (a) *while the saturation* $n(Z,T)$ *of the absorber is presented in* (b). *Note the formation and splitting of the pulse on the left-hand side and center of the computational domain. For this value of the gain g, the saturable absorber recovers sufficiently to allow for the existence of a second and third pulse on the computational domain chosen.*

use the parameters $\tau = 0.1$, $\gamma = 0.6$, $e_A = 10$, $n_0 = 0$, $g = 0.87$, and $T_d = 5$ which gives a 1-picosecond recovery time for the saturable absorber. For these parameters, stable mode-locking is shown to occur. The stability of the mode-locking is highly sensitive to the parameters chosen, especially the value of g, which gives a delicate balance between the gain and loss. Slightly lower values of the gain g lead to decay of solutions to zero, whereas higher values of g result in multiple pulse per round trip configurations such as that shown in Figure 6. For these simulations, the computational domain is critical. Specifically, the saturable absorber dynamics (9) whose solution is given by (10) is calculated on a finite computational domain (for the example in Figure 6, $T \in [-10, 10]$) versus the theoretical limit of $T \in [-\infty, \infty]$. The result of this is shown in both Figures 5 and 6. Specifically, the pulses arrange themselves in the cavity so that the maximum gain is achieved. In Figure 5, the pulse formation occurs on the left edge of the computational domain. This allows the gain to almost completely recover and the total integrated gain from the saturable absorber is maximized over the computational domain. Larger computational domains help alleviate the problem of a shifting pulse position. However, this comes at the expense of significantly larger computational times since (9) must be integrated for every time step when computing solutions of (8). Ideally, the computational domain should be chosen to be much longer than the normalized decay time, in this case chosen to be $T_d = 5$. For physically reasonable values of $T_d = 20$, the domain will need to be chosen very large indeed. Regardless of this computational issue, it is difficult in general to find stable mode-locked solutions due to the delicate balance required in the gain-loss dynamics and its sensitivity to changes in the parameters. This drawback is offset by the physically realistic saturable absorber model with a slow recovery dynamics.

2.4. Quintic Ginzburg–Landau Models. One can build on the master mode-locking models pioneered by Haus by considering the quintic complex Ginzburg–Landau equation (or complex Swift–Hohenberg equation). This model is a phenomenological model for a wide variety of physical phenomena. In particular, the complex Ginzburg–Landau equation arises as a generic description of the onset of instability in nonequilibrium physical systems [45]. In the context of mode-locking,

it is a simple extension of the cubic and quintic master mode-locking models already considered. The generic evolution in this case is given by [41, 42, 43]

$$(11)\quad i\frac{\partial Q}{\partial Z}+\left(\frac{1}{2}-i\tau\right)\frac{\partial^2 Q}{\partial T^2}-i\kappa\frac{\partial^4 Q}{\partial T^4}+(1-i\beta)|Q|^2Q+(\nu+i\sigma)|Q|^4Q-i\gamma Q=0.$$

The governing evolution is similar to (6) with a constant gain (7b). However, there are differences. Specifically, (11) includes a fourth-order diffusion term with strength κ, which models a quartic contribution to the gain bandwidth. Additionally, there is a quintic self-phase modulation term with strength ν which results in a nonlinear phase shift.

Unlike the cubic master mode-locking model or the saturable absorber model of the last subsection, stable localized solutions are abundant in (11). The parameter space is also large due to the number of coefficients which can be varied and the various nonlinear terms. This leads to a large number of solutions which remain localized but which can have a much richer variety of spatial-temporal dynamics. Of course, it is difficult to make a connection between this model and physical mode-locking systems, i.e., there no longer exists a direct link between the nonlinear coefficients and experiment. Specifically, the parameters β, σ, and ν are, by construction, only qualitative in nature. Regardless, the merit of (11) is in generating a large and interesting class of so-called *dissipative solitons* [41, 42, 43].

To illustrate a small subset of the spatial-temporal dynamics, (11) is simulated in different parameter regimes. Figure 7 shows four distinct behaviors present in the system. In Figure 7(a) a phenomenon referred to as *exploding solitons* is observed [41]. In this simulation, the evolution first settles to a localized pulse which periodically *explodes* and reforms to the localized pulse. This occurs periodically in the system and is robust under perturbation. Indeed, this periodic spatial-temporal dynamics is an attractor to (11). A more typical breather-like behavior is observed in Figure 7(b). This shows a continuous, periodic variation in the pulse shape which again is stable under even large perturbations. Interestingly enough, this periodic breather has been shown to undergo a period doubling instability toward chaos when the cubic gain/loss parameter β is increased [41]. Figure 7(c) is similar to 7(b) but with the exception that the dynamics is not periodic. In fact, the oscillations grow in width with a changing period in distance Z. In this parameter regime, both drift and periodic variations in the pulse center position have been observed [41]. Finally, Figure 7(d) demonstrates the formation of a localized, steady-state multihump solution to (11). The number of humps on the solution are strongly dependent upon the initial conditions, i.e., there are more humps for higher initial values of the L^2 norm ($\|Q\|^2$). Unlike the previous examples which have spatial-temporal dynamics, this simply settles to a steady-state solution [42]. The parameters used for the simulations in Figure 7 are given in Table 1.

Given the qualitative nature of this model, it is difficult to claim a correspondence between the simulations and a physical mode-locked laser. However, many of the key ingredients in the laser cavity are captured from this qualitative viewpoint. Indeed, some evidence even exists for the case of the exploding solitons of Figure 7(a) [46]. Regardless of the correspondence and physical relevance, the behaviors observed in (11) make it worthy of further study. Certainly, little or nothing is known analytically of the stability of the steady-state solutions and the spatial-temporal breathers of the system. Although difficult to approach from an analytic framework, numerical linear stability analysis techniques prove to give insight into the underlying instability and periodicity mechanisms observed [41, 42, 43].

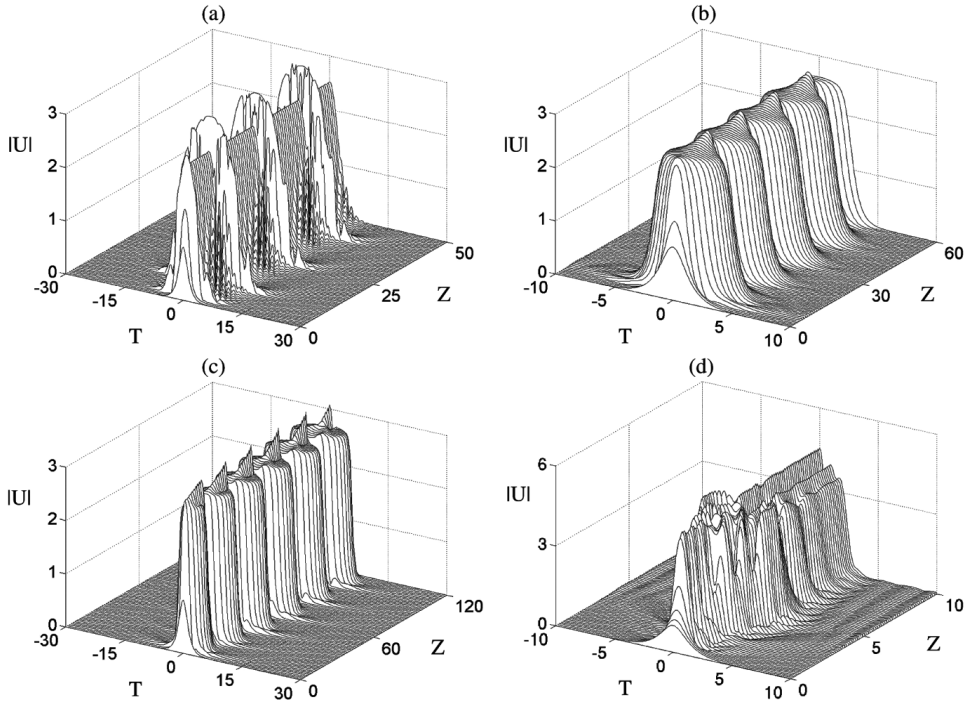

Fig. 7 *Subset of four possible behaviors found in* (11). *In* (a), *the formation of an* exploding soliton *is observed where the localized pulse solution periodically undergoes "explosions" before returning to the localized solution. Both* (b) *and* (c) *appear to give rise to localized breather type solutions. In* (b), *the breather is periodic over a single width oscillation. In* (c), *the breather is not periodic. Rather, the pulse width grows in distance* Z. *The formation of a multihump steady state is shown in* (d), *where the number of peaks is determined by the initial cavity energy, i.e., the* L^2 *norm. The parameter values used for these simulations are shown in Table* 1.

Table 1 *Parameters used in the four simulations* (a), (b), (c), *and* (d) *of Figure* 7.

Figure 7	τ	κ	β	ν	σ	γ
(a)	0.125	0	1.0	−0.6	−0.1	−0.1
(b)	0.08	0	0.66	−0.1	−0.1	−0.1
(c)	0.08	0	0.835	−0.8	−0.11	−0.1
(d)	−0.3	−0.05	1.6	0	−0.1	0.5

3. Quantitative Mode-Locking Models: Experimentally Realized. Unlike the models presented in the previous section, the models presented in this section aim to be of a quantitative nature. Thus an effort is made to include all the relevant physical effects present in a given mode-locked laser. As will be demonstrated by the various models, there are many ways to achieve the intensity-dependent discrimination required for mode-locking. And by modeling the system from a quantitative perspective, a realistic model can be obtained for a given laser cavity configuration. This allows for a characterization of the model which is beyond the generic qualitative

approach. In particular, the breakdown of the mode-locking behavior and the optimal laser performance can be investigated.

The first step in these models is to consider the quantitative effects of the pulse propagation in the absence of a mode-locking mechanism. Thus we begin by once again considering the pulse propagation in the optical fiber (or a solid-state configuration [4]) in the absence of a mode-locking term (e.g., $\beta = 0$ in (3)). Thus the governing evolution is given by

$$i\frac{\partial Q}{\partial Z} + \frac{1}{2}\frac{\partial^2 Q}{\partial T^2} + |Q|^2 Q + i\gamma Q - ig(Z)\left(1 + \tau\frac{\partial^2}{\partial T^2}\right)Q = 0, \tag{12}$$

where Q represents the electric field envelope normalized by the peak field power $|Q_0|^2$. Here the variable T represents the physical time in the rest frame of the pulse [6, 7] normalized by $T_0/1.76$, where T_0 is the FWHM of the pulse (e.g., $T_0 =$ 200 fs). The variable Z is scaled on the dispersion length $Z_0 = (2\pi c)/(\lambda_0^2 \bar{D})(T_0/1.76)^2$ corresponding to the average dispersion. The parameter $\bar{D}$ (in ps/km-nm) gives the average normal ($\bar{D} < 0$) or anomalous ($\bar{D} > 0$) dispersion in the laser cavity. This gives the one-soliton peak field power $|Q_0|^2 = \lambda_0 A_{\text{eff}}/(4\pi n_2 Z_0)$. Further, for all models discussed $n_2 = 2.6 \times 10^{-16}$ cm^2/W is the nonlinear coefficient in the fiber, $A_{\text{eff}} = 60$ μm^2 is the effective cross-sectional area of the fiber, $\Gamma = 0.2$ dB/km is the fiber loss, and $\lambda_0 = 1.55$ μm and c are the free-space wavelength and speed of light, respectively. For a gain bandwidth which can vary from $\Delta\lambda = 20$–40 nm, we find that $\Omega = (2\pi c/\lambda_0^2)\Delta\lambda$ so that τ varies from $\approx 0.08 - 0.32$ for a pulse width of $T_0 = 200$ fs. τ is the parameter which largely controls the resulting pulse width of the stabilized mode-locked pulse stream since it limits the spectral gain bandwidth of the mode-locking process. Note that this model differs from the experimental setup for which up to three fiber segments are utilized with differing dispersion values and effective cross-sectional areas (see Figure 1(b)). Although corrections to the average dispersion can be included, numerical results suggest that they can be neglected with only a minimal amount of error incurred [47, 48]. The gain in the fiber is incorporated through the dimensionless parameter $g = g(Z)$ just as in (4).

In addition to (12), an accurate model is required for the mode-locking mechanism. Certainly every parameter in (12) has a direct correlation to an experimentally measurable physical value. Thus it remains only to provide a quantitatively accurate model of the mode-locking mechanism to achieve an accurate and physically realizable model for the mode-locked laser cavity. In the subsections that follow, various models for the mode-locking mechanism will be considered and shown to generate stable mode-locked pulse trains.

3.1. Mode-Locking with Saturable Absorption. The master mode-locking model considered the saturable absorption as a phenomenological nonlinear gain/loss term in (3). A more quantitative and comprehensive model of the SBR dynamics requires a description of the microscopic interactions between the intracavity radiation and the quantum well structure, and, consequently, extensive numerical modeling [49, 50, 51, 52]. Here we simply incorporate the mode-locking action of the SBR via an empirical model of its nonlinear temporal response. A typical SBR structure consists of a broadband AlAs/GaAs Bragg reflector and two uncoupled InGaAs/InP quantum wells. The complete structure has a $\approx 99.5\%$ saturated reflectivity at 1.55 μm with a bandwidth of ≈ 150 nm [53]. Since the optical field penetrates through only several microns in the SBR structure, we ignore the effects of the material dispersion in the Bragg reflector, and we model the steady-state SBR nonlinear reflectivity

response as a jump condition attached to the propagation equation (12). The model includes a *fast* component representative of the virtual carrier transitions (AC Stark) and a *slow* component representative of the real transitions that incorporates a saturated term and a slow relaxation time [50, 51, 52]. Thus the combined response can be described by the jump condition [53]

$$Q_+ = \left[1-\sigma_l - \sigma_f\left(1-\frac{|Q_-|^2}{|Q_-|^2_{max}}\right) - \sigma_s\left(1-\frac{\int_{-\infty}^{T}|Q_-|^2dT}{\|Q_-\|^2}\right.\right.$$
$$\left.\left.\times\exp\left(-\mathrm{H}(T-T_{max})\frac{T-T_{max}}{T_d}\right)\right)\right]Q_- = f(|Q_-|)\,Q_-, \tag{13}$$

where $Q_\pm$ denotes the pulse before (–) and after (+) the SBR interaction, T_d is the decay time of the SBR slow response which is normalized on T_0, σ_l is the intrinsic loss of the SBR, σ_f measures the relative strength of the instantaneous SBR response, and σ_s measures the relative strength of the corresponding slow saturation response. Note that $|Q(T_{max})| = |Q|_{max}$ gives the power maximum and its relative position, and $\mathrm{H}(T-T_{max})$ is the standard Heaviside function [54] for which $\mathrm{H}(T-T_{max}) = 0$ for $T - T_{max} < 0$ and $\mathrm{H}(T-T_{max}) = 1$ for $T - T_{max} > 0$. The jump condition (13) is a phenomenological idealization of the steady-state interaction dynamics of the SBR with the electric field. Physically, the SBR is capable only of responding to the instantaneous power rather than the integrated power ($\|Q\|^2$) and maximum power ($|Q|^2_{max}$) as per (13). In addition to the convenient mathematical description, (13) can provide a quantitatively correct leading-order model for the SBR dynamics. Thus the SBR action is localized to the temporal window of the pulse, i.e., far from the pulse the radiation experiences $\approx 2\%$ absorption. This is in contrast to the master mode-locking equation [11] and soliton mode-locking models [26] for which radiation far from the localized pulse can experience nearly $\approx 100\%$ absorption.

Time-resolved pump-probe measurements of the reflectivity have been made on an SBR sample at 1.55 microns. In this case it is observed that both a slow and a fast response are present. Thus for a hyperbolic secant pulse ($Q_- = \eta\,\mathrm{sech}\,wT\exp(i\Theta(Z,T))$) inserted in (13), we can compare this simple model with the experimental findings obtained via pump-probe measurements. Figure 8 depicts the comparison between the experimental and analytic results of (13), where w is chosen to match a ≈ 400 fs FWHM pulse, $T_d = 14$ ps$/T_0$ (a 14 ps decay time), $\sigma_l = 0.005$ for a saturated reflectivity of 99.5%, and $\sigma_f = \sigma_s = 0.65\sigma$, where σ is the maximum change in reflectivity of the SBR. Note the excellent agreement between the simple analytic model given by (13) and the experimental results. We estimate from experiments that the maximum change in reflectivity is $\approx 2\%$. This gives $\sigma = 2\%$ and $\sigma_f = \sigma_s = 1.3\%$. These parameter values for the SBR will be used in the numerical and analytical calculations that follow. We expect the simple jump condition (13) to model the SBR dynamics only for well-behaved, near steady-state mode-locking, i.e., a single pulse per round trip configuration.

The SBR dynamics can be incorporated into the propagation equation (12) for the pulse evolution in the fiber. The model derived is not simply a heuristic or qualitative model, but rather an asymptotically valid model for the nonlinear pulse dynamics. Thus, a direct comparison between the averaged evolution, which resembles the usual master mode-locking equation (Ginzburg–Landau equation), the full dynamics given by (12), (4), and (13), and the experimental results can be made. The averaged evolution incorporates the effect of the SBR and output coupler by implementing

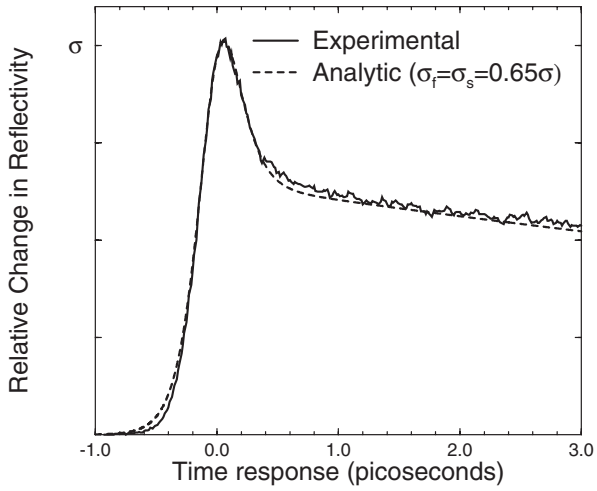

Fig. 8 *Comparison of the experimental pump and probe measurements of the SBR at* 1.55 μm *with the jump condition of* (13) *which includes a fast response and a slow saturation response with relaxation.*

them continuously over the fiber segment [53]. The averaged evolution equation for the pulse dynamics is given by

$$i\frac{\partial Q}{\partial Z} + \left(\frac{D}{2} - i\tau g(Z)\right)\frac{\partial^2 Q}{\partial T^2} + i(\tilde{\gamma} - g(Z))Q + \left(\alpha - i\frac{\sigma_f}{|Q|^2_{max}}\right)|Q|^2 Q$$
$$- i\sigma_s \frac{\int_{-\infty}^{T} |Q|^2 dT}{\|Q\|^2} \exp\left(-\mathrm{H}(T - T_{max})\frac{T - T_{max}}{T_d}\right) Q = 0, \tag{14}$$

where $\tilde{\gamma} = \gamma + 1 - R + \sigma_l + \sigma_f + \sigma_s$. Equation (14) is similar to the master mode-locking equation. However, there are significant differences due to the addition of the slow response with relaxation, the fast response scaling $\sigma_f/|Q|^2_{max}$, and the contribution of linear parts in $\tilde{\gamma}$ proportional to σ_l, σ_f, and σ_s. Equation (14) is valid under the condition that the pulse amplitude does not change significantly per round trip [53].

Equation (14) admits exact solutions in certain asymptotic parameter regimes. For the case in which the SBR response has no slow response, i.e., $\sigma_s = 0$, chirped solutions take the form of (5) [34]. For $\sigma_s \neq 0$, there is no longer an exact solution of (14). However, in the physically relevant limit for which $\sigma_s \ll 1$, the slow response term can be treated as a perturbation to the $\sigma_s = 0$ case. In particular, we examine the case for which there is no relaxation (e.g., $T_d = \infty$) and consider the traveling wave solution

$$Q(Z, T) = \eta[\operatorname{sech} w(T - vZ)]^{1+iA} \exp(i\phi(Z)). \tag{15}$$

As in the case with $\sigma_s = 0$, the parameters η, w, ϕ, and A satisfy the previous algebraic equations with the additional restriction that $v(1+iA) = (\sigma_s/2w)(1+\coth w(T-vZ))$, which cannot be satisfied unless $v = 0$ and $\sigma_s = 0$, i.e., the case of no slow response considered previously. However, for the case in which $v \ll 1$ and $T - vZ \gg 1$, we find $v \approx \sigma_s/w$. So although no solutions exist, we obtain a crude estimate for the leading-order drift of the pulse due to the slow response. In addition to the

approximate traveling wave solution found above, care must be taken when comparing the analytic solution with the numerical results of the full equation, which includes the slow response and relaxation. In particular, the value of σ_s in the definition of $\tilde{\gamma}$ must be modified in order to account for the effective loss due to the slow response. Simply setting $\sigma_s = 0$ gives pulse solutions which are much too large because the value of g_0 calculated numerically takes into account the loss due to a nonzero σ_s. The effective slow response can be found by averaging the slow response so that $\bar{\sigma}_s \approx 0.65\sigma_s$ [53].

For mode-locking in the normal dispersion regime, the experimental laser cavity consists of three fiber segments of lengths 13 cm, 19 cm, and 95 cm with dispersion values of 17.0 ps/km-nm, −9.1 ps/km-nm, and −51.6 ps/km-nm, respectively (see Figure 1(b)). Thus the cavity length is 127 cm with an average cavity dispersion of $\bar{D} \approx -38$ ps/km-nm. It should be noted that the −9.1 ps/km-nm (19 cm) segment is the erbium-ytterbium gain fiber. The saturated intracavity power measured experimentally is $e_0 = 21.3$ mW, which is achieved with a specific value of g_0. Finally, we assume the erbium-ytterbium fiber has a 25 nm FWHM gain bandwidth. For mode-locking in the anomalous regime, the laser cavity is comprised of three fiber segments of lengths 24 cm, 17 cm, and 49 cm with dispersion values of 17.0 ps/km-nm, −9.1 ps/km-nm, and 17.0 ps/km-nm, respectively. The cavity length is then 90 cm ($Z_{\text{cav}} = 180$ cm) with an average dispersion value of $\bar{D} \approx 12$ ps/km-nm. In this case the output coupling is 2% and the intracavity power is estimated from measurements to be ≈ 10 mW. In addition, we take an effective fiber bandwidth (FWHM) of ≈ 45 nm. Although this bandwidth is broader than that of the 20–25 nm erbium-ytterbium fiber, it is a reasonable assumption given that the pulse propagates a majority of the time in essentially bandwidth-unlimited fiber. Thus the larger bandwidth allows the self-phase modulation to have a stronger broadening effect in the fiber cavity. All other parameters, including $\sigma_f = \sigma_s = 1.3\%$ and $\sigma_l = 0.5\%$, remain as in the normal dispersion case.

The governing evolution as given by (12) and (13) results in the dynamics illustrated in Figure 9. In Figures 9(a) and 9(b) a typical simulation shows the time domain and spectrum of mode-locking in the normal regime. Here the pulse settles to a ≈ 13.5 ps (FWHM) pulse. In contrast, Figures 9(c) and 9(d) depict the mode-locking in the anomalous regime. In this case, the pulse locks to a ≈ 500 fs (FWHM) pulse, which is consistent with experimental estimates. The spectral evolution in this case clearly shows the formation of a highly chirped pulse in the normal regime. The accuracy of the numerical and analytic models can be tested by comparing in Figure 10 experimental results with the governing equations (12) and (13), the averaged equation (14), and the analytic approximations (15). This model was the first to provide a direct quantitative comparison between theory and experiment. The agreement achieved is remarkable. However, the jump condition (13) is rather cumbersome and lacks the elegance and simplicity desired for significant mathematical analysis. Thus the accurate mode-locking description incurs obvious setbacks.

3.2. Mode-Locking with an Acousto-optic Modulator. In contrast to the passive mode-locking models represented in the previous two subsections, this subsection considers the mode-locking dynamics driven by active mode-locking techniques. The active modulation model of mode-locking is fundamentally different from the previous subsections in that instead of a passive, nonlinear response generating pulse shaping, here it is a linear, time-dependent, periodic forcing which results in stabilized pulses. This periodic forcing generates peaks and troughs in the gain as a function of the time T. Thus cavity energy will accumulate at the local peaks of the gain, whereas

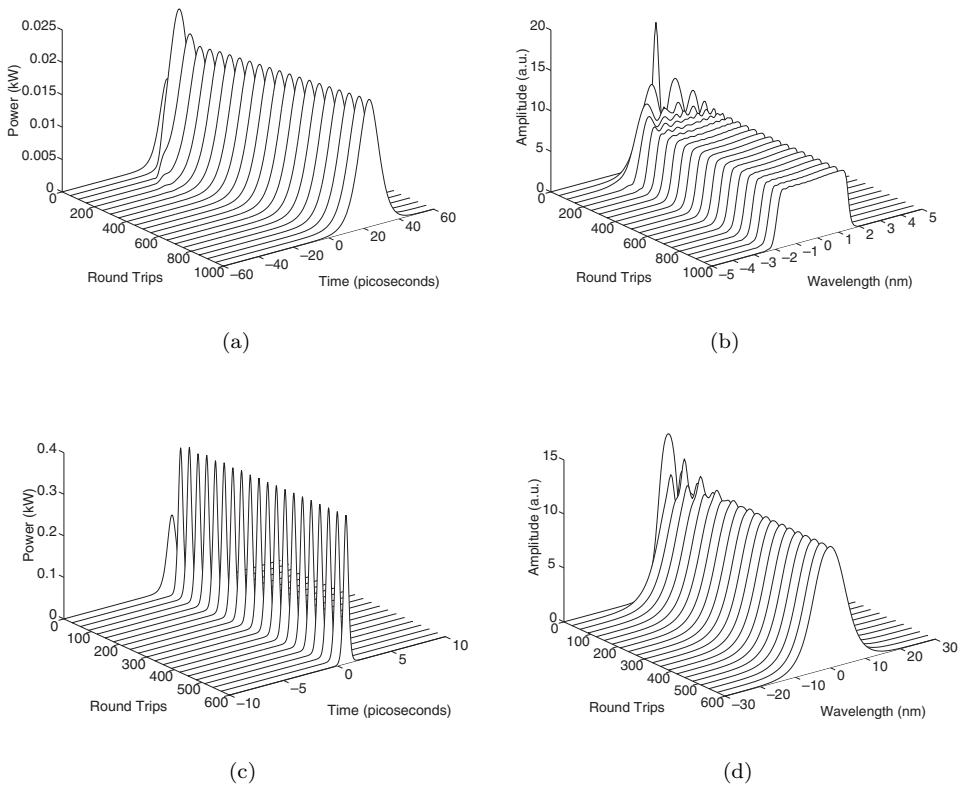

Fig. 9 *Numerical simulation of the pulse evolution as governed by* (12) *and* (13) *in both the time* (a) *and frequency domain* (b) *for a fiber cavity with an average defocusing (normal) dispersion value of* $\bar{D} = -38.1$ *ps/km-nm. In* (a) *the pulse is seen to mode-lock to a* ≈ 13.6 *ps chirped pulse whose spectral evolution is given by* (b). *Numerical simulation of the pulse evolution in both the time* (c) *and frequency* (d) *domain for a fiber cavity with an average focusing (anomalous) dispersion value of* $\bar{D} \approx 12$ *ps/km-nm. In* (c) *the laser is seen to mode-lock to a* ≈ 420 *fs chirped pulse with a time-bandwidth product of* ≈ 0.4 *and whose spectral evolution is given by* (d).

cavity energy will be attenuated at the local troughs in the gain. Similar to saturable absorption, this preferential localization of cavity energy gives the necessary pulse shaping required to form and stabilize localized pulses in a periodic wavetrain.

The pulse evolution in the actively mode-locked, optical fiber laser system is governed by the equation [26, 27, 55]

$$(16)\quad i\frac{\partial Q}{\partial Z} + \frac{1}{2}\frac{\partial^2 Q}{\partial T^2} + |Q|^2 Q - ig(Z)\left(1+\tau\frac{\partial^2}{\partial T^2}\right)Q + iM(\Gamma - \mathrm{cn}^2(\omega T, k))Q = 0,$$

where the normalizations in (12) are assumed and τ again controls the gain bandwidth. The parameters M, Γ, and ω measure the normalized strength and frequency of the active modulation element which is responsible for generating the mode-locked pulse stream. The gain in the fiber is incorporated through the dimensionless parameter $g = g(Z)$ just as in (4). We have generalized the periodic forcing to a Jacobi elliptic [56] cosine function $\mathrm{cn}^2(\omega T, k)$ [55]. Here $0 \le k \le 1$ is the elliptic modulus. In the limit

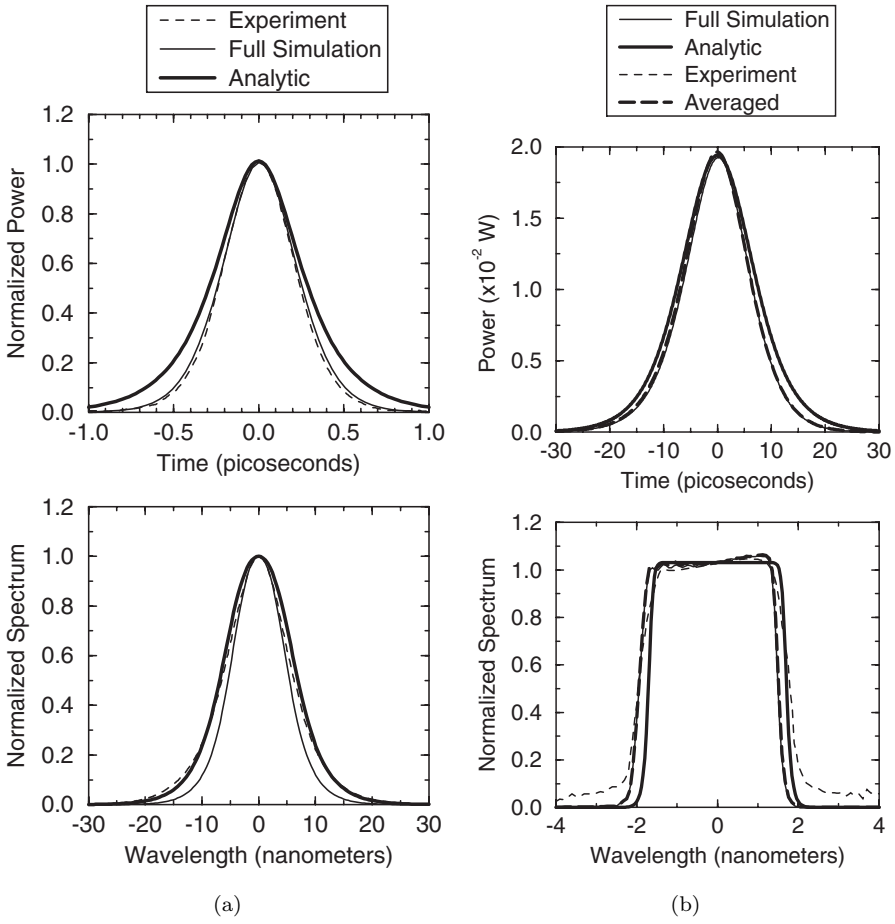

Fig. 10 *Comparison of results from experiment with those from the governing equations* (12) *and* (13) *illustrated in Figure* 9*, the averaged equation* (14)*, and the analytic approximations* (15)*. Note the remarkable agreement between all three models and the experimental results. In* (a)*, the experimental anomalous mode-locking (light dashed) is compared with Figure* 9(c)–(d) *(light solid), whereas* (b) *depicts the experimental normal mode-locking (light dashed) in comparison with Figure* 9(a)–(b) *(light solid).*

$k = 0$, the modulation reduces to a purely sinusoidal forcing as given previously [26, 27]. For values of $k < 0.9$ the gain modulation is virtually indistinguishable from the sinusoidal modulation. However, as $k \to 1^-$, the modulation becomes a series of well-separated hyperbolic secants. In practice, the acoustic modulator creates a periodic modulation of the gain. Generally it is assumed that this modulation is of a sinusoidal nature [26, 27]. However, the freedom in choosing the elliptic modulus k allows for the consideration of much more general modulation formats, including well-separated periodic gain peaks. These additional modulation formats, although not strictly of the Jacobi elliptic form, have the potential of generating a broader class of mode-locked pulse train solutions which are perturbatively close to the $\mathrm{cn}^2(T, k)$ considered here.

The introduction of the Jacobi elliptic functions allows one to proceed analytically. Specifically, analytic solutions to (16) with a constant gain parameter $g(Z) = g =$

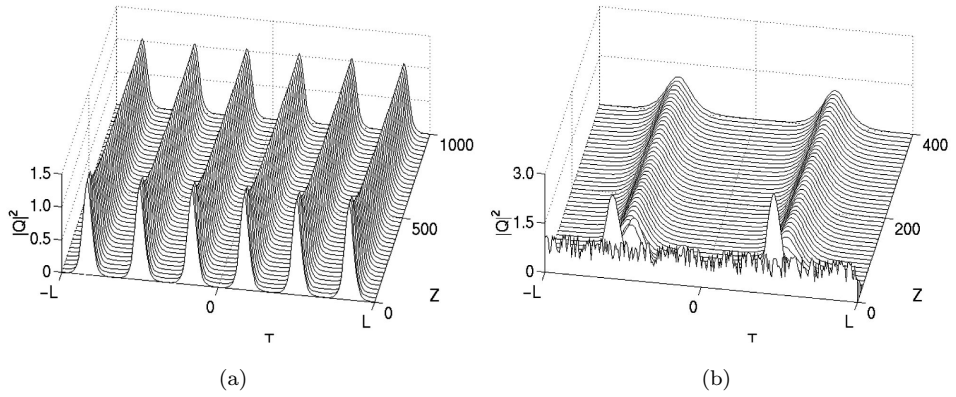

(a) (b)

Fig. 11 (a) *Stable evolution of the mode-locking pulse train starting near the exact solution given by* (17). *Here the initial amplitude is perturbed from the exact solution by* 0.2. *Three periods are considered with the parameters used being* $k = 0.999$, $g = 0.3$, $\tau = 0.1$, *and* $T \in [-L, L]$, *where* $L = 12\int_0^{\pi/2} d\alpha/\sqrt{1 - k^2 \sin^2 \alpha}$. (b) *Stable evolution of the mode-locking pulse train starting with initial noise. One period is considered with the parameters used being* $k = 0.999$, $g = 0.3$, $\tau = 0.1$, *and* $T \in [-L, L]$, *where* $L = 4\int_0^{\pi/2} d\alpha/\sqrt{1 - k^2 \sin^2 \alpha}$. *Note the formation of two pulses from this noise realization.*

constant are found. In particular, two families of solutions exist. The first takes the form (setting $\omega = 1$ without loss of generality)

$$Q(Z, T) = k\,\mathrm{cn}(T, k)\exp[-i(1/2 - k^2)Z]\,, \tag{17}$$

where $M = -2k^2 g\tau$ and $\Gamma = (2k^2 - 1/\tau - 1)/2k^2$. This solution branch represents a periodic train of pulses where adjacent pulses are separated by a node. This nodal separation is critical to the stability of the pulse trains, i.e., adjacent pulses need to be out-of-phase in order to be stabilized. Alternatively, an in-phase solution is found of the form

$$Q(Z, T) = \mathrm{dn}(T, k)\exp[-i(k^2/2 - 1)Z]\,, \tag{18}$$

where $M = -2k^2 g\tau$ and $\Gamma = k^2(2\tau(1 - 1/k^2) + 1/k^2 + \tau(2 - k^2)/k^2)/2$. This solution branch represents a periodic train of pulses where adjacent pulses are not separated by a node. Such solutions are found to be unstable [55].

The behavior of both the out-of-phase and in-phase pulse train evolutions is depicted in Figures 11 and 12. Figure 11 illustrates the stabilizing influence of the active modulation on out-of-phase solutions, whereas Figure 12 demonstrates the unstable evolution of both an in-phase solution and a lower k value out-of-phase solution [55]. The stabilized pulse train of Figure 11 settles quickly into the exact solution given by (18). For both these simulations, the elliptic modulus was $k = 0.999$ so that the localized solutions are nearly hyperbolic secant pulses. In this case, there is a node between neighboring pulses and only an exponentially small interaction exists between pulses. In contrast, Figure 12 shows that lower k values of out-of-phase solutions are destabilized by pulse-to-pulse interactions and in-phase solutions decay to zero.

The model for the active modulation is detailed elsewhere [55]. Its primary strength is in providing a model for studying the full pulse train as opposed to a

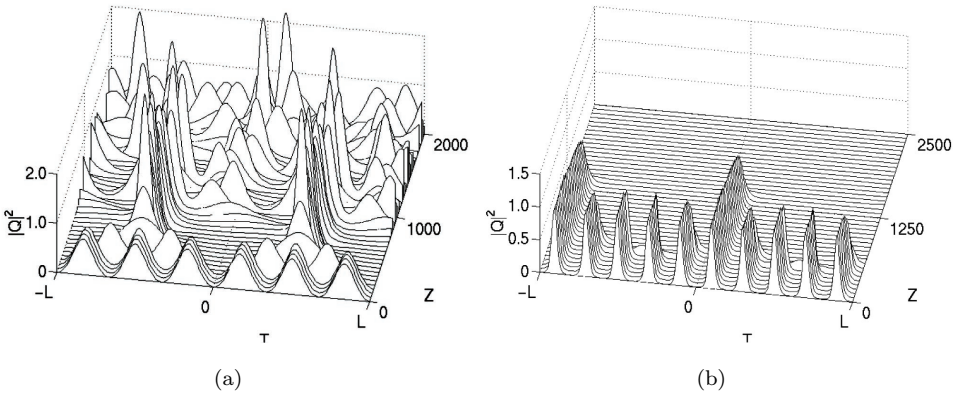

(a) (b)

Fig. 12 (a) *Unstable evolution of the mode-locking pulse train starting near the out-of-phase solution given by* (17). *Three periods are considered with the parameters used being* $k = 0.75$, $g = 0.3$, $\tau = 0.1$, *and* $T \in [-L, L]$, *where* $L = 12\int_0^{\pi/2} d\alpha/\sqrt{1-k^2\sin^2\alpha}$. *In contrast to Figure* 11, *the reduced separation of the neighboring pulses causes the pulses to destabilize and evolve to a chaotic pulse train.* (b) *Evolution of the mode-locking pulse train starting near the in-phase solution given by* (18) *with* $k = 0.999$ *and* $T \in [-L, L]$, *where* $L = 20\int_0^{\pi/2} d\alpha/\sqrt{1-k^2\sin^2\alpha}$. *Here we begin with the exact solution and show that it decays to zero. Thus in-phase solutions are unstable.*

single isolated pulse. In particular, the well-separated limit ($k \to 1$) gives rise to stable out-of-phase pulse train solutions. Many instabilities arise in the mode-locked system, such as the phenomenon of Q-switching, which are difficult to characterize with single pulse models such as those presented in the previous two subsections. Thus, the model allows for a more comprehensive investigation of the interaction dynamics in a mode-locked pulse stream since exact solutions are available for analytic and computational study. The major drawback to active mode-locking is the limited repetition rates available using acousto-optic (electronic) modulators, i.e., most other optical mode-locking models allow for significantly higher repetition rates.

3.3. Mode-Locking with a Passive Polarizer. For applications where polarization effects are important, one must consider a system of coupled nonlinear Schrödinger equations (CNLS). Despite the loss of integrability [57], soliton-like solutions are still found to persist [58, 59]. The two key modeling elements describing the mode-locking dynamics are the inclusion of nonlinear polarization rotation induced by the cross-phase modulation, and polarization control through the passive polarizer. In particular, we model optical pulses with CNLS subject to periodic perturbations by the passive polarizer. This model allows us to examine the underlying mode-locking mechanism of the fiber ring laser of Figure 1(a). The primary objective is to determine the performance characteristics of the laser, i.e., the uniformity of the resulting pulse train.

The evolution of the slowly varying envelope of the electric field in an optical fiber subject to chromatic dispersion, Kerr nonlinearity, and polarization effects is given by the system of CNLS [59]

$$i\frac{\partial U}{\partial Z} + \frac{1}{2}\frac{\partial^2 U}{\partial T^2} - KU + \left(|U|^2 + A|V|^2\right)U + BV^2U^* = 0\,, \tag{19a}$$

$$i\frac{\partial V}{\partial Z} + \frac{1}{2}\frac{\partial^2 V}{\partial T^2} + KV + \left(A|U|^2 + |V|^2\right)V + BU^2V^* = 0\,. \tag{19b}$$

Here the governing interactions are among the chromatic dispersion, the cubic Kerr nonlinearity, and the fiber birefringence (measured by the variable K). We have scaled the equation as in (12). Asymmetry of the nonlinear coupling requires the relation $A+B=1$ to be satisfied by the dielectric coefficients A and B [59, 60, 61]. Although a wide range of values may be considered for the coefficients, we focus on the particular case for which $A = 2/3$ and $B = 1/3$, which are the physical values specific to the Kerr nonlinearity.

The CNLS can be recast as a variational principle by defining the appropriate Lagrangian [59, 62, 63]. We are interested in investigating the evolution of pulses generated by a mode-locking fiber laser. Based upon physical observations [15, 16, 17, 18], we assume that these pulses are approximately described by an amplitude and width fluctuation, η, a polarization angle, P, a relative phase, ψ, a total phase, ϕ, and a quadratic chirp, β, which are related to the U and V fields by

$$U = \sqrt{I\eta}\,\operatorname{sech}(\eta T)\,\cos P\,\exp[-i\psi/2 + i\beta T^2 + i\phi/2]\,, \tag{20a}$$

$$V = \sqrt{I\eta}\,\operatorname{sech}(\eta T)\,\sin P\,\exp[+i\psi/2 + i\beta T^2 + i\phi/2]. \tag{20b}$$

Here, we denote the initial energy contained within the pulse by I. In addition, we assume that these pulse parameters depend solely on Z. Following [62], we impose that the variational derivatives of the Lagrangian with respect to P, ψ, η, and β are zero, and we obtain

$$\frac{dP}{dZ} = \frac{1}{3}BI\eta\sin(2P)\sin(2\psi)\,, \tag{21a}$$

$$\frac{d\psi}{dZ} = -\frac{4}{3}BI\eta\cos(2P)\sin^2(\psi) + 2K\,, \tag{21b}$$

$$\frac{d\eta}{dZ} = -2\beta\eta\,, \tag{21c}$$

$$\frac{\pi}{2}\frac{d\beta}{dZ} = \eta^4 - \pi^2\beta^2 - I\eta^3\left[1 - B\sin^2(2P)\sin^2(\psi)\right]. \tag{21d}$$

This system of coupled ordinary differential equations models the leading-order pulse characteristics governed by the CNLS (19) as long as the pulse remains close to the ansatz given in (20). Extensive numerical simulations have been done to verify that the evolution of the pulse's characteristics governed by (19) are well approximated by (21) [62]. This reduction from (19) to (21) is a significant simplification of the mathematical model of the fiber laser. Note that when strong dispersion fluctuations are present in the cavity, a modulational instability can occur which modifies the localized pulse solution description [64].

We model the optical fiber loop laser shown in Figure 1(a) using (21) in a periodic domain corresponding to the loop length L. After a pulse propagates once around the fiber loop, it interacts with the polarizer. This polarizer attenuates the components of the pulse that are not aligned with the polarizer angle, Θ, resulting in a net rotation of the pulse's polarization state and a reduction of the pulse's amplitude, η. Afterward, erbium-doped fiber amplifiers boost the pulse's power back to the original cavity energy. Thus the polarizer and amplifier combination act as a periodic perturbation on the pulse dynamics described by (21). To simplify the modeling, we consider this

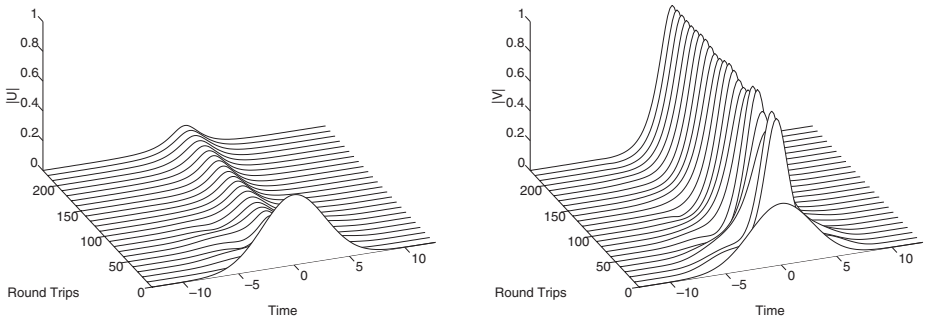

Fig. 13 *Stable mode-locking evolution of the governing CNLS* (19) *with a passive polarizer. In this case we consider the parameters* $\Theta = 0.45\pi$ *and* $K = 0.1$*. Although the amplitude appears to lock to a constant value, we note that a detailed look after each round trip of the cavity shows amplitude fluctuations on the order of* 4%*.*

combination of polarizer and amplifier to be one operation that acts instantaneously after each round trip. This assumption is valid when the losses of each round trip are small [62]. Furthermore, we assume that the original input power is conserved throughout the laser so that this operation preserves power and is simply a rotation of the polarization state.

We define the polarizer angle, Θ, to be the angle between the alignment of the passive polarizer and the fast U-axis. This convention is consistent with the definition of P and leads to the jump condition at the polarizer [62]

$$P_+ = \tan^{-1}\left[\alpha \tan\left(P_- - \Theta\right)\right] + \Theta, \tag{22}$$

where $P_\pm$ are the polarization angles before $(-)$ and after $(+)$ the polarizer. The polarizer strength parameter, α, indicates the efficiency of the polarizer in attenuating components not aligned with the polarizer angle Θ. To be consistent with physical values, we consider $\alpha = 0.01$ so that the polarizer attenuates 99% of the pulse not aligned with the polarization angle. A typical example of the mode-locking behavior is given in Figure 13, which shows that an arbitrary localized initial condition quickly settles to an amplitude-locked solution. For this computation, $\Theta = 0.45\pi$ and $K = 0.1$.

Since we can control the polarization state by aligning it with the passive polarizer ($P \approx \Theta$), the reduced description (21) suggests that setting the polarizer angle to $\Theta = 0$ or $\Theta = \pi/2$ results in stable mode-locking operation [63]. Near $\Theta = 0$ and in the absence of the polarizer, the underlying fiber evolution is unstable. However, the action of the polarizer stabilizes the dynamics by continually forcing the polarization state to be near $P = 0$. Provided the polarizer acts on a sufficiently fast scale in comparison with the soliton evolution length, nearly uniform pulse trains can be realized. We illustrate this pulse propagation behavior in Figure 14(a), where we demonstrate the evolution of the primary quantity of interest η. By detuning the polarizer from $\Theta = 0$, large, quasi-periodic fluctuations result in the dynamics. This instability occurs despite the fact that the polarization state is locked on a value near $P = 0$. A similar behavior occurs for $\Theta \approx \pi/2$. Figure 14(b) illustrates the pulse train amplitude behavior as the polarizer is detuned from the slow axis.

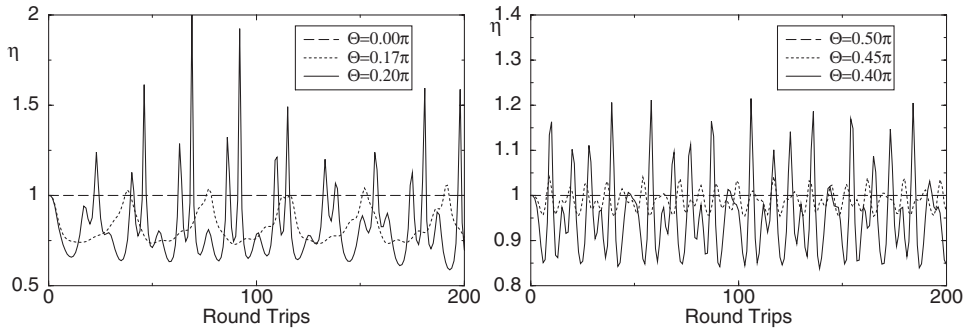

Fig. 14 *Pulse train uniformity (η fluctuations) over* 200 *round trips of the fiber cavity with* $K = 0.10$, $B = 1/3$, $I = 1$. (a) *As the polarizer is detuned from* $\Theta = 0$, *the amplitude fluctuations increase and the pulse train uniformity is destroyed.* (b) *Similarly, as the polarizer is detuned from* $\Theta = \pi/2$, *the amplitude fluctuations increase and the pulse train uniformity is destroyed. However, the uniformity here is not as severely affected as detuning from* $\Theta = 0$

.

Thus four parameters are essential in understanding the resulting pulse train uniformity in a birefringent optical fiber with a periodic rotation of the polarization state due to a passive polarizer: the polarization (P), phase (ψ), amplitude (η), and chirp (β). Although the phase and polarization are irrelevant experimentally, these two parameters are essential in determining the pulse train uniformity via nonlinear coupling to the amplitude and chirp. The reduced model also allows for the discovery of three stable operating regimes of the mode-locked laser [63]. Further, it suggests that mode-locking near the fast- and slow-axes is crucial for achieving a uniform pulse train. Indeed, control of the polarizer and birefringence strength (K) can be used to tune the laser center-frequency [65]. Although this model is capable of capturing the polarization dynamics, it does not include the energy equilibration of the previous models, i.e., the energy is assumed to be constant in the model. However, once saturated mode-locking operation is established, the model is important in determining the resulting polarization-locked soliton train dynamics. It should be noted that polarization-locking can also be achieved in lasers mode-locked with saturable absorbers [66, 67].

4. Quantitative Mode-Locking Models: Theoretically Proposed. This section continues with the quantitative modeling aspects of the mode-locking behavior. However, the focus here is on mode-locking configurations and devices which have yet to be realized experimentally. With the emergence of new fabrication technologies and the continued development of optical materials, many of the proposed models are promising candidates for cheap, robust, and reliable mode-locking technologies. Indeed, next-generation laser sources are expected to emerge from the continued theoretical and computational understanding of current day mode-locked lasers.

As with the quantitative models of the previous section, the basic modeling of the laser cavity starts with (12). It remains then to develop a quantitatively accurate model for the intensity discrimination device responsible for generating mode-locking. In the subsections which follow, specific models are proposed for the devices responsible for intensity discrimination. Physically realistic values for these devices

are considered and their suitability for mode-locking evaluated. Three of the mode-locking models considered in this section are driven by a nonlinear mode-coupling interaction [28]. The fundamental principle in each of these models centers on the nonlinear mode-coupling which resonantly couples low intensity light to a second mode which is attenuated. In contrast, high intensity light is detuned from resonance and largely unattenuated during propagation. This provides the necessary intensity discrimination for generating mode-locked soliton pulses for a large range of parameter space.

4.1. Mode-Locking with an LPFG. Fiber gratings have long been used for photonic applications. For instance, an LPFG can be used as a band-rejection filter for all-optical signal processing [68] or as a mode-locking element in a laser cavity. The concept of the LPFG as a mode-locking mechanism arises from the intensity-dependent mode-coupling which occurs between copropagating core and cladding modes [69]. Nonlinear mode-coupling was first investigated by Jensen [70] for copropagating core modes in the context of a dual-core, nonlinear directional coupler. This nonlinear dual-core coupler was later proposed by Winful and Walton [71] as a mechanism for generating stable mode-locked pulses [71, 72]. The underlying concept is as follows: a resonant and linear mode-coupling interaction transfers energy periodically between core and cladding modes [73]. Nonlinearity, however, can be used to detune the resonant interaction by shifting the propagation constant of each mode via the self-phase and cross-phase modulation introduced by the nonlinearity [69, 70]. Thus the LPFG can be manufactured so that a resonant linear interaction occurs between the core mode and a given cladding mode. Then the low intensity parts of a pulse which propagate through the grating are efficiently coupled to the cladding and attenuated. In contrast, the peak of the pulse is detuned from the resonant coupling (i.e., the transmission minimum of the LPFG is shifted to longer wavelengths) and is transmitted more efficiently. Thus, the wings of a pulse are attenuated slightly more than its peak, giving the necessary pulse shaping required to achieve stable mode-locked operation after many round trips of the fiber laser cavity. The numerical model presented here is based on the fiber laser configuration of Figure 1(c). The ideal laser cavity consists of a segment of optical fiber ($\approx$ 1 m), an output coupler ($\approx$ 2%), a reflector, and a short section of the LPFG ($\approx$ 5–10 cm). This simple passive device is sufficient for producing stable mode-locked pulse trains.

The asymptotic derivation of the nonlinear coupled mode equations for the copropagating core and cladding modes in an LPFG are carried out in Kutz et al. [74]. This derivation assumes quasi-monochromatic waves along with the paraxial and rotating-wave approximations. These asymptotic assumptions are justified for the LPFGs under consideration. To induce coupling between copropagating modes, the grating period is adjusted so that a resonant interaction occurs between the core mode and a given cladding mode. Each cladding mode will have a particular coupling strength with the core mode. Thus the index of refraction of the grating is given by

$$n(X, Y, Z) = n_0(X, Y)\left[1 + \Delta n_{uv} \cos(\gamma Z)\right], \tag{23}$$

where $n_0(X, Y)$ accounts for the transverse index profile of the grating and Δn_{uv} measures the ultraviolet induced index of refraction change in the grating in the longitudinal direction. Since the grating is periodic, we assume there is a dominant Fourier mode component which measures the period of the grating. Thus the parameter γ measures the grating period which is crucial for the copropagating coupling.

As derived previously [74], the coupling between copropagating core mode U (i) and cladding mode V (j) is given by

$$i\frac{\partial U}{\partial Z} + (c_{ii}|U|^2 + 2c_{ij}|V|^2)U + d_{ij}V - \frac{\Delta}{2}U = 0, \tag{24a}$$

$$i\frac{\partial V}{\partial Z} + (2c_{ij}|U|^2 + c_{jj}|V|^2)V + d_{ij}U + \frac{\Delta}{2}V = 0, \tag{24b}$$

where the normalized nonlinear and linear coupling coefficients are given by

$$c_{ij} = \frac{4\pi^2 n_2}{\lambda A_{\text{eff}}} \frac{(|\phi_{i0}|^2, |\phi_{j0}|^2)_r}{(|\phi_{10}|^2, |\phi_{10}|^2)_r} Z_0 |E_0|^2, \tag{25a}$$

$$d_{ij} = \frac{\Delta n_{\text{UV}} \pi}{2\lambda} (V(r)\phi_{i0}, \phi_{j0})_r \, Z_0, \tag{25b}$$

and the parameter

$$\Delta = [\gamma - (\beta_i - \beta_j)/2k] \; Z_0 \tag{26}$$

measures the detuning from resonant coupling ($\Delta = 0$). Note that the indices i and j determine the specific modes to be coupled. Since we are interested in coupling the single-core mode to the cladding, $i = 1$. The index j can take on values for any of the cladding modes. Typically there are hundreds of cladding modes so that j can easily range from 2 to 100. The parameters β_j are the propagation constants. It will be assumed in the simulations which follow that resonant coupling between copropagating modes can be achieved. The nonlinearity acts to shift the resonance for high intensity pulses so that they are transmitted through the grating with a minimal amount of coupling to the cladding.

The linear coupling strength, which is proportional to the ultraviolet induced index changes, is given by the parameter d_{ij}. The parameters c_{ii} and c_{jj} give the strength of the self-phase modulation acting on the core and cladding modes, respectively. Similarly, the parameter c_{ij} measures the strength of the cross-phase modulation between the core and cladding. At sufficiently high intensities, the self-phase and cross-phase modulation terms act to shift the transmission minimum of the grating to longer wavelengths by inducing an intensity-dependent phase shift.

The pulse shaping provided by the LPFG is demonstrated by simulating (24) for various pulse shapes and intensities. This gives a clear picture of the dynamics of both the core and cladding mode dynamics and energy therein. For illustrative purposes, we assume the grating length to be $Z = 0.7$, which corresponds to a grating of length 11.76 cm for the scalings given for (12). Further, we take the normalized linear and nonlinear coupling values to be $d_{14} = 2$, $c_{11} = c_{44} = 0.3$, and $c_{14} = 0.5$. The propagation of an initial Gaussian core mode pulse with an amplitude of $a = 4$ is demonstrated in Figure 15. Note that after passing through the grating, the initial pulse is narrowed considerably while energy is exchanged with the cladding mode. Since the peak of the pulse is detuned from resonance due to its intensity, it does not couple energy to the cladding. The input and output pulse shapes for the cladding and core modes are shown in Figure 16. This shows the pulse narrowing process in greater detail.

The pulse shaping which occurs due to the interaction of the core and cladding modes in the LPFG can lead to stable mode-locking in the laser cavity [75]. Figure 17

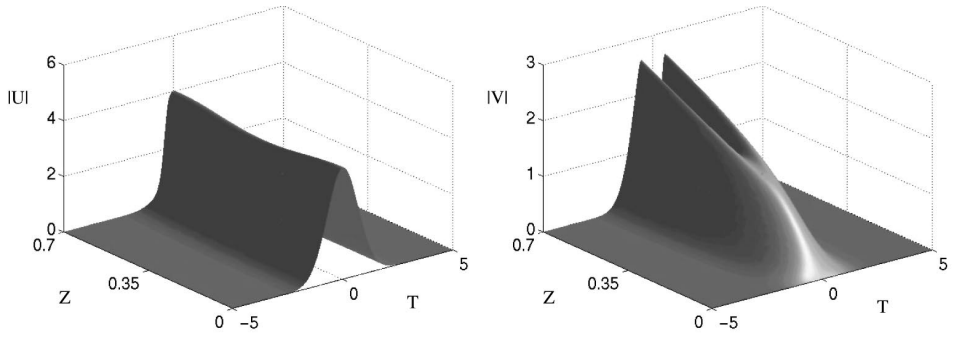

Fig. 15 *Evolution of an initial Gaussian core mode pulse profile over a grating of length* $Z = 0.7$ *with a computational domain of* $L = 5$ *and coupling coefficients* $d_{14} = 2$, $c_{11} = c_{44} = 0.3$, *and* $c_{14} = 0.5$.

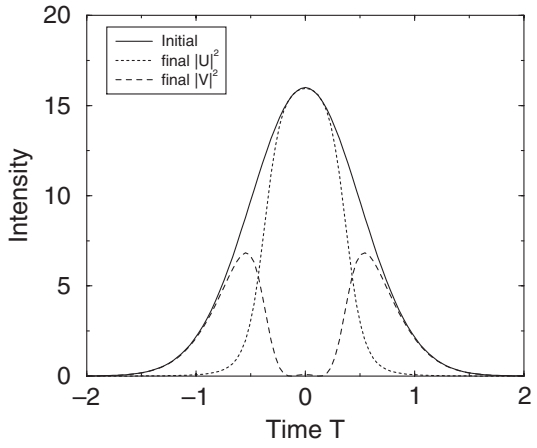

Fig. 16 *Input and output pulse profiles through a grating given an initial Gaussian core mode pulse profile propagated over a grating of length* $Z = 0.7$ *with a computational domain of* $L = 5$ *and coupling coefficients* $d_{14} = 2$, $c_{11} = c_{44} = 0.3$, *and* $c_{14} = 0.5$.

demonstrates this stable mode-locked operation. In this case, we have taken a fiber laser cavity that is 1 meter in length and inserted a very short LPFG of length $Z = 0.1$ with linear and nonlinear coupling coefficients $d_{14} = 12$, $c_{11} = c_{44} = 0.2$, and $c_{14} = 20$. Additionally, the gain parameter is taken to be $g_0 = 1$ in (4). A full cavity simulation includes propagation in the fiber according to (12) and (4) with propagation through the LPFG (24) twice per round trip (see Figure 1(c)). In this case, the cavity mode-locks the pulse after roughly 15 round trips of the cavity. The corresponding cladding field is also depicted. Note that most of the energy transfer from core to cladding occurs on the wings, thus giving the necessary pulse shaping for mode-locking. Further recall that this cladding field is then strongly attenuated once coupling back to the fiber cavity occurs.

Other behaviors also occur in the cavity. In particular, the gain parameter g_0 acts as a bifurcation parameter for the pulse dynamics. Figure 18 depicts the evolution of

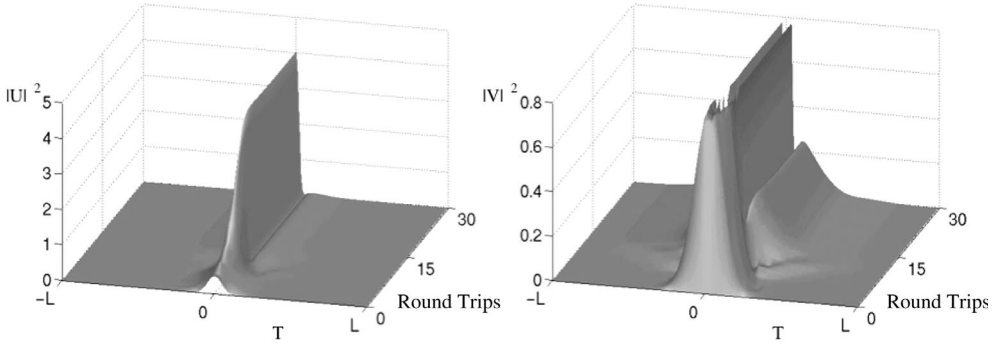

Fig. 17 *Stable mode-locking pulse dynamics for a laser cavity with a grating length* $Z = 0.1$ *and fiber length of* 1 *meter. Here the coupling coefficients are* $d_{14} = 12$, $c_{11} = c_{44} = 0.2$, *and* $c_{14} = 20$ *with a computational domain* $2L = 50$. *The gain parameter in this case is* $g_0 = 1$.

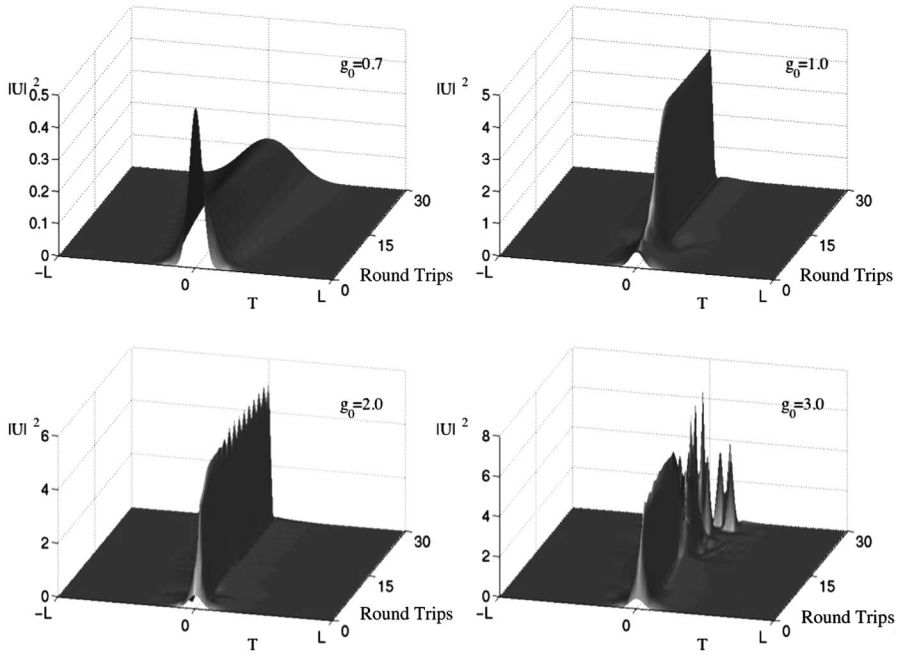

Fig. 18 *Pulse dynamics for a laser cavity with a grating length* $Z = 0.1$ *and fiber length of* 1 *meter. Here the coupling coefficients are* $d_{14} = 12$, $c_{11} = c_{44} = 0.2$, *and* $c_{14} = 20$ *with a computational domain* $2L = 50$. *The gain parameter in this case varies among* $g_0 = 0.5, 1.0, 2.0$, *and* 3.0. *Note that close to the ideal cavity gain* ($g_0 \approx 1$) *the cavity stabilizes and mode-locks a pulse.*

the pulse with the gain parameter being $g_0 = 0.5, 1.0, 2.0$, and 3.0. If the cavity gain is too low ($g_0 = 0.5$), the pulse slowly dies in the cavity and there is no mode-locking. For larger values of gain ($g_0 = 1.0$) the pulse shaping allows for the stabilization of a mode-locked pulse. Higher values of gain generate periodic mode-locked trains or chaotic pulse trains, neither of which are typically desirable for application purposes.

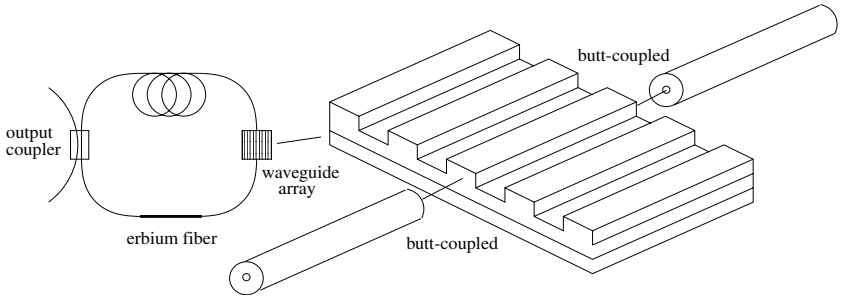

Fig. 19 *Configuration of a mode-locked laser cavity based upon a waveguide array element for intensity discrimination. The waveguide array is a set of periodically spaced waveguides which couple evanescently to nearest neighbors* [76, 77, 78, 79, 80]. *Only the energy which remains in the original launch waveguide is of interest in the mode-locking, i.e., the energy in the neighboring waveguides is lost.*

4.2. Mode-Locking with Waveguide or Fiber Arrays. Waveguide arrays have recently been of great interest due to their application to all-optical signal processing and switching. The particular interest here is in the phenomenon which occurs through evanescent mode-coupling [73]. The linear mode-coupling in conjunction with nonlinear self- and cross-phase modulation effects has been proposed [76] due to a wide variety of soliton-like effects and dynamics [76, 77, 78, 79, 80]. The particular application of mode-locking considered here relies on the intensity-dependent mode-coupling much like the LPFG laser of the previous subsection (see Figure 19 for the mode-locked laser configuration).

The equations which govern the nearest neighbor coupling of the waveguides are given by [76, 77, 78, 79, 80]

$$(27)\quad i\frac{dA_n}{dZ} + (A_{n-1} + A_{n+1}) + \gamma|A_n|^2 A_n = 0 \qquad (n = -N, \ldots, -1, 0, 1, \ldots, N),$$

where A_n represents the electric field amplitude in the nth waveguide and we have rescaled the equations so that the coupling coefficient is unity. Note that there are a total of $2N + 1$ waveguides. It has been assumed that the waveguide array is periodically spaced and lossless. The waveguide spacing is fixed so that nearest neighbor linear coupling dominates the interaction between waveguides. Further, the waveguide material is assumed to have a cubic nonlinearity and a sufficient number of waveguides so that no spatial boundary effects occur in the dynamics.

A typical representation of the grating array is shown in Figure 19. The array is inserted into an optical fiber ring cavity as the mode-locking element responsible for generating intensity-dependent discrimination in a propagating temporal pulse. A simple simulation of (27) serves to illustrate the dynamics of the waveguide array. By butt-coupling the fiber to the waveguide array, electromagnetic radiation initially enters only into a single waveguide of the array. We denote this initial waveguide as A_0. The initial energy in A_0 will couple through nearest neighbor interactions to adjacent waveguides. These will in turn couple to their neighbors. Figure 20 demonstrates the effective spatial diffraction of energy in the waveguide array for two different initial conditions and for $\gamma = 1$. In the first (left panel), the initial field $A_0 = 1$ so that the nonlinearity has little effect on the linear coupling dynamics. For higher initial intensities (right panel), i.e., $A_0 = 3$, the nonlinearity provides self-focusing which

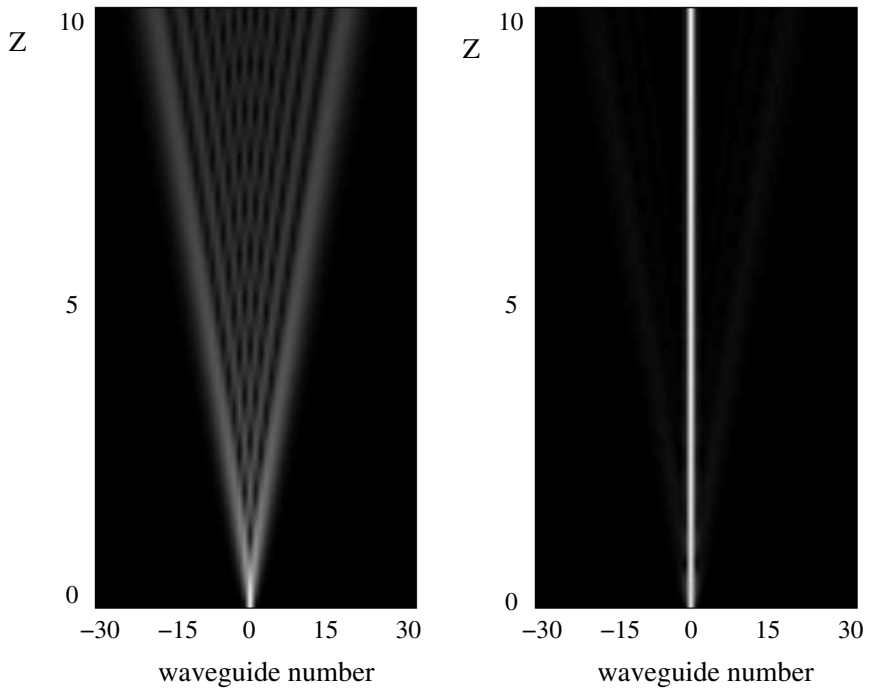

Fig. 20 *Mode-coupling dynamics in the waveguide array as given by* (27) *with* $\gamma = 1$. *For both figures, energy is launched into the center waveguide with amplitude* $A_0 = 1$ *(left) and* $A_0 = 3$ *(right). For the lower intensities, the energy is quickly coupled to the neighboring waveguides and diffracted throughout the structure. For higher intensities, the energy remains highly localized in the launch waveguide with only a small portion escaping to the neighboring waveguides.*

helps to confine the initial energy to the launch waveguide. Only a small amount of energy is coupled to the neighboring waveguides in this case.

A simple understanding of this localization comes from thinking of (27) as a finite-difference discretization of the NLS (1), i.e., the second-order finite-difference discretization of the second derivative couples to nearest neighbors. Thus the effective diffraction equation in the continuum limit is a *spatial* NLS in the waveguide array [76]. For weak nonlinearity, diffractive spreading occurs so that the energy propagates away from the center waveguide. However, when diffraction and self-phase modulation are balanced, a steady-state soliton profile in the spatial direction is achieved and energy remains localized in the launch waveguide.

As with the LPFG, the temporal pulse shaping aspects of the waveguide array are what determine the suitability of the array for mode-locking [81]. To illustrate the analogue of Figure 16 for the LPFG, a temporal initial condition is launched into the waveguide array subject to (27). Figure 21 illustrates the pulse shaping which occurs for a train of two noisy initial Gaussian pulses. The light solid lines are the initial data while the heavy lines represent the output of the center waveguide. Note that the low amplitude pulse is strongly coupled out to the neighboring waveguides and lost, whereas the high intensity pulse is subject to strong self-phase

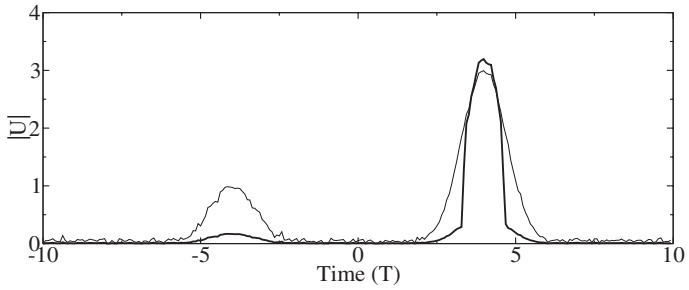

Fig. 21 *Temporal input (light lines) and output (heavy lines) in the center waveguide A_0 after propagation through the waveguide array of Figure* 20*. Note the required pulse shaping which occurs for higher intensities versus lower intensities.*

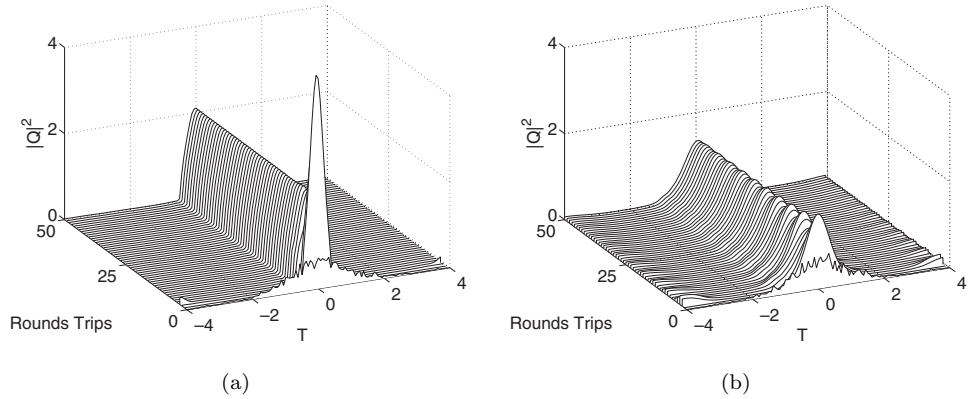

Fig. 22 *Stable mode-locking dynamics using* (a) *a waveguide array and* (b) *a dual-core fiber. For this case, a* 5 *m fiber cavity is considered with either a* 6 *mm waveguide* (a) *or a* 10 *cm dual-core fiber* (b) *as the mode-locking element. A* 20% *coupling loss is assumed at the input and output of the mode-locking element and a gain of* $g_0 = 0.7$ (a) *and* $g_0 = 0.39$ (b) *is taken in* (4)*. Additional parameters assumed are* $\tau = 0.1$*,* $\gamma = 0.1$*,* $e_0 = 1$*, and the coupling parameters given by Figures* 21 *and* 25 *for* (a) *and* (b)*, respectively.*

modulation and remains localized in the center waveguide. Note further that the higher intensity pulse is substantially narrowed in the time domain, as is expected of a mode-locking mechanism.

In summary, the basic principle of mode-locking operation relies on the same ideas as the LPFG mode-locked laser. The waveguide array via mode-coupling provides the necessary intensity discrimination which allows stable mode-locked pulses to be supported in the ring cavity of Figure 19. A typical example is illustrated in Figure 22(a) for a 5-meter fiber cavity with a 6-millimeter waveguide array. An additional 20% loss is taken at the input and output of the waveguide array due to coupling losses. Note that a fiber array [82] would work in almost an identical fashion to the waveguide array.

4.3. Dual-Core Fiber Laser. Yet another example of mode-locking induced by mode-coupling arises from dual-core optical fibers. In principle, the mode-locking mechanism is identical to that of the LPFG and waveguide array, i.e., high inten-

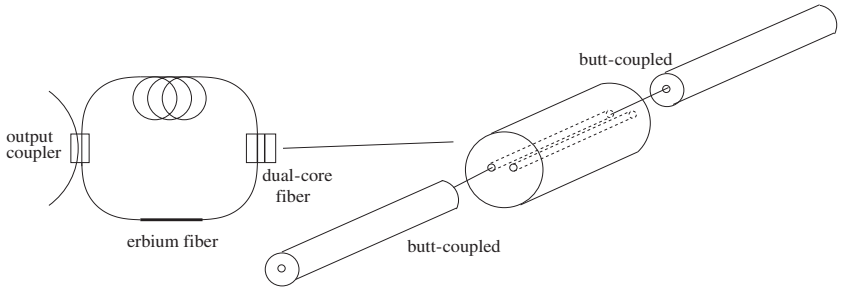

Fig. 23 *Configuration of a mode-locked laser cavity based upon a dual-core fiber for intensity discrimination. The dual-core fiber couples via evanescence from core to core* [73]. *Only the energy which remains in the original launch core is of interest in the mode-locking, i.e., the energy in the second core is lost.*

sity portions of a pulse are almost completely transmitted in one core of the fiber, whereas low intensity portions are coupled to the second core and lost. A typical cavity configuration is illustrated in Figure 23. For proper design of the laser, it is important to engineer the dual-core fiber spacing and length so that in the *linear* regime electromagnetic energy is completely coupled from one core to its neighbor. This coupling, as in the waveguide array, is an evanescent mode-coupling. Thus low intensity portions of a pulse will be effectively attenuated and the appropriate intensity discrimination is established. Note that for longer fibers, energy from the second core will begin coupling back to the original core mode.

The normalized equations which govern the nearest neighbor coupling of the waveguides are given by [70, 73]

$$i\frac{dA_1}{dZ} + A_2 + \gamma|A_1|^2A_1 = 0, \tag{28a}$$

$$i\frac{dA_2}{dZ} + A_1 + \gamma|A_2|^2A_2 = 0, \tag{28b}$$

where A_n $(n = 1, 2)$ represents the electric field amplitude in the two cores, and we have rescaled the equations so that the coupling coefficient is unity. It has been assumed that the dual-core fiber is lossless.

A simulation of (28) serves to illustrate the dynamics of the dual-core coupling. Initially, electromagnetic radiation enters only into a single core A_1. The initial energy in A_1 will couple through evanescent wave interaction to the neighboring core mode A_2. Figure 24 demonstrates the effective spatial exchange of energy in the dual-core fiber for two different initial conditions and for $\gamma = 1$. In the first (left panel), the initial field $A_1 = 1$ so that the nonlinearity has little effect on the linear coupling dynamics. For higher initial intensities (right panel), i.e., $A_1 = 3$, the nonlinearity provides self-focusing which helps to confine the initial energy to the launch core mode. Only a small amount of energy is coupled to the neighboring core mode in this case.

As with the LPFG and waveguide array lasers, the temporal pulse shaping aspects of the dual-core coupling are what determine the suitability of the dual-core fiber for mode-locking. To illustrate the analogue of Figures 16 and 21 of the LPFG and waveguide array, a temporal initial condition is launched into the waveguide array subject to (28). Figure 25 illustrates the pulse shaping which occurs for a train of two noisy initial Gaussian pulses. The light solid lines are the initial data while the

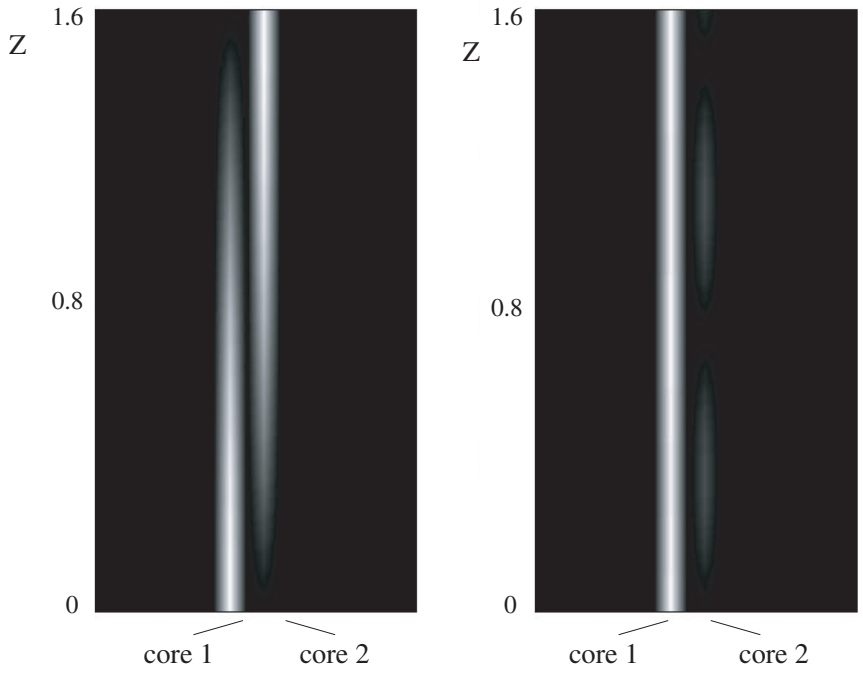

Fig. 24 *Mode-coupling dynamics in the dual-core fiber as given by* (28) *with* $\gamma = 1$. *For both figures, energy is launched into the left core with amplitude* $A_1 = 1$ *(left) and* $A_1 = 3$ *(right). For the lower intensities, the energy is coupled evanescently to the second core. For higher intensities, the energy remains highly localized in the launch waveguide with only a small portion escaping to the second core.*

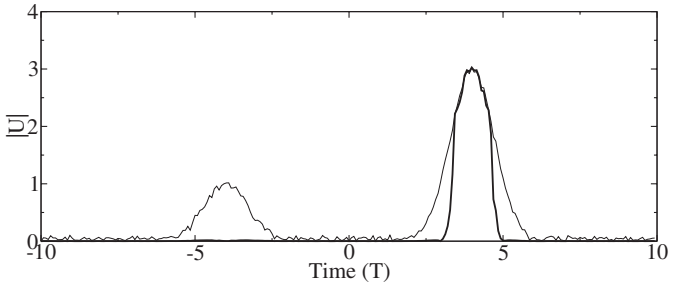

Fig. 25 *Temporal input (light lines) and output (heavy lines) in the launch core* A_1 *after propagation through the dual-core fiber of Figure* 23. *Note the required pulse shaping which occurs for higher intensities versus lower intensities.*

heavy lines represent the output of the launch core. Note that the low amplitude pulse is strongly coupled out to the neighboring core and lost, whereas the high intensity pulse is subject to strong self-phase modulation and remains localized in the launch core. Note further that the higher intensity pulse is substantially narrowed in the time domain, as is expected of a mode-locking mechanism.

In summary, the basic principle of mode-locking operation relies on the same ideas as the LPFG and waveguide array mode-locked lasers. The dual-core array via mode-coupling provides the necessary intensity discrimination which allows stable mode-locked pulses to be supported in the ring cavity of Figure 23. Although the model is theoretically capable of supporting mode-locked pulse operation, practical issues limit the usefulness of the dual-core mode-locked laser. Most important is the fact that the fiber length required to achieve complete coupling of *linear* energy from one core to the next is on the order of several meters or more. However, over this length, the dual-core fiber is highly sensitive to temperature and core-to-core spacing perturbations. These perturbations greatly affect the mode-coupling dynamics and pose practical limitations on generating mode-locked pulses in the cavity. However, with the advance of material technologies such as chalcogenide glass [83, 84], the core-to-core spacing in the dual-core fiber can be decreased in order to shorten the dual-core fiber length significantly. And with the increased nonlinearity provided by the chalcogenide glass, the self-phase modulation remains sufficiently strong to provide the necessary pulse shaping over very short distances of dual-core fiber. The need for chalcogenide glass is also necessary in the LPFG in order to keep the grating to lengths of tens of centimeters. Thus the key components of a physically realizable dual-core fiber based mode-locked laser can be achieved. A typical example is illustrated in Figure 22(b) for a 5-meter fiber cavity with a 10-centimeter dual-core fiber. An additional 20% loss is taken at the input and output of the waveguide array due to coupling losses. It should be noted that the mode-locked lasers discussed in the last three subsections, which are based upon nonlinear mode-coupling interactions, have not been realized experimentally.

4.4. Mode-Locking with Parametric Amplifiers. As an alternative to erbium-doped amplifiers, the use of phase-sensitive amplifiers (PSAs) for compensating the linear loss in the laser cavity can be considered. PSAs have been suggested since they are free of spontaneous emission noise and are ideal quantum limited amplifiers with a 0 dB noise figure [85]. PSAs thus do not themselves contribute to the Gordon–Haus timing jitter [86] (although some quantum noise is still present due to the linear fiber loss). Generally speaking, PSAs amplify light with light. In particular, phase-sensitive gain can be provided to an optical signal by an optical pump pulse through the process of parametric amplification [87]. As a result, the components of the signal pulse which are *in-phase* with the pump pulse are amplified, while *out-of-phase* components are attenuated. Specifically, by decomposing an input signal into quadratures (orthogonal complex phases)

$$Q = (A + iB)\exp(i\phi/2), \tag{29}$$

the action of the PSA is to amplify components which are in-phase (A) with the amplifier and attenuate those which are out-of-phase (B):

$$Q_+ = [A_- \exp(\alpha) + iB_- \exp(-\alpha)]\exp(i\phi/2)\,. \tag{30}$$

Here the $\pm$ denotes the input field before and after an amplifier, α is the field gain of the amplifier, and ϕ is the reference phase associated with the PSA pump field. Thus the in-phase portion is amplified and the out-of-phase portion is attenuated. This attenuation of the out-of-phase portion works to eliminate phase variations across the signal pulse's profile, which in turn leads to its enhanced stability [88, 89].

Pulse propagation through an optical fiber which includes dispersion, nonlinearity, linear loss, and periodic phase-sensitive amplification is governed by the perturbed

NLS [88, 89]

$$i\frac{\partial Q}{\partial Z}+\frac{1}{2}\frac{\partial^2 Q}{\partial T^2}+|\,Q\,|^2 Q+i\frac{\Gamma}{\epsilon}Q-i\frac{1}{\epsilon}h\left(\frac{Z}{\epsilon}\right)Q-i\frac{1}{\epsilon}\,e^{i\phi(Z)}\,f\left(\frac{Z}{\epsilon}\right)Q^*=0, \tag{31}$$

where Γ is the linear loss rate in the fiber and the rapidly varying periodic functions h and f account for the effect of the optical phase-sensitive gain of the lumped amplifiers [88, 89]. Thus

$$h(\zeta)Q=[\cosh(\beta|P|z_a)-1]\sum_{n=1}^{N}\delta(\zeta-nl)Q(nl^-,T)\,, \tag{32}$$

$$f(\zeta)Q^*=\sinh(\beta|P|z_a)\sum_{n=1}^{N}\delta(\zeta-nl)Q^*(nl^-,T)\,. \tag{33}$$

Here z_a is length of the PSA, l is the laser cavity length in terms of ζ, P is the pump amplitude, β is a real constant which depends upon the $\chi^{(2)}$ nonlinearity of the amplifying medium and frequency of the mode-locked signal, and N is the total number of round trips in the laser cavity. The phase of the amplifier is represented by $\phi(Z)$ and the scalings are those used in (12). Here the amplifier spacing (cavity length) Z_l is assumed to be much shorter than the dispersion length Z_0. Mathematically, this assumption is made by defining $\epsilon\equiv Z_l/Z_0\ll 1$ [88, 89].

Performing a multiple-scale averaging [90, 91] of (31) using the short length scale $\zeta=Z/\epsilon$, the dispersion length scale Z, and the long length scale $\bar{\xi}=\epsilon Z$ gives the following fourth-order evolution equation [88, 89]:

$$U_\xi+\frac{1}{4}\left(\frac{\partial^2}{\partial T^2}-\kappa\right)^2 U-\Delta\alpha\,U-\kappa U^3+U^5+3BU\left(\frac{\partial U}{\partial T}\right)^2+(B+1)U^2\frac{\partial^2 U}{\partial T^2}=0, \tag{34}$$

where $B=(2-\tanh\Gamma/\Gamma)$, $\kappa=d\phi/dZ$, $\xi=\bar{\xi}/(2\tanh\Gamma)$, $\Delta\alpha$ is an $O(\epsilon^2)$ correction to the exact balance between loss and gain in the cavity propagation, and U is the scaled in-phase component of the pulse envelope after each amplifier, namely,

$$U=\left(\frac{1-e^{-2\Gamma}}{2\Gamma}\right)^{1/2}\Re e(Qe^{-i\phi/2}). \tag{35}$$

Equation (34) is a fourth-order, nonlinear, diffusion equation which governs the pulse dynamics over the long length scale ξ. The parameter $\Delta\alpha$ represents an $O(\epsilon^2)$ deviation from the exact balance of loss and gain which accounts for a small necessary amount of overamplification [89]. In a mathematical context, $\Delta\alpha$ is a scaled version of the Floquet exponent produced by the linear loss and periodic amplification when the dispersion and nonlinearity are neglected. The parameter κ, which represents a constant amplifier phase rotation rate ($\kappa=d\phi/dZ$), can be taken to be unity without loss of generality since it can be scaled out of (34). Therefore, $\kappa=1$ for the remainder of this section. The amplitude rescaling corresponds to normalizing the pulse envelope so that $\int U^2\,dT$ is the average pulse energy over one cavity period [88, 89]. Although the evolution equation (34) inherits much of its structure from the NLS, it is important to note that the evolution is non-Hamiltonian in nature, and, therefore, its dynamics are those of a dissipative system.

An idea of the general structure of the solutions to (34) can be obtained by considering $\Gamma=0$. In this limit,

$$U_0=\eta\,\mathrm{sech}\,\eta T, \tag{36}$$

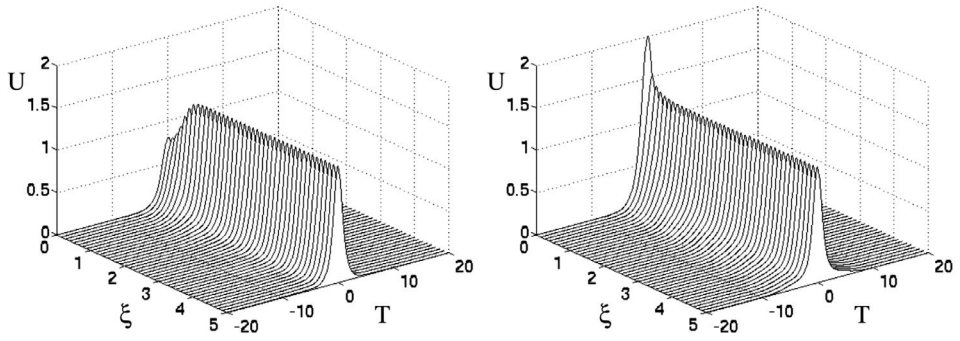

Fig. 26 *Numerical simulation of* (34) *showing exponential decay of initial transients to the stable steady-state hyperbolic secant solution for* $\Delta\alpha = 0.1$. *Two initial conditions are represented, one below the stable branch (left) and a second above (right).*

where $\eta = (1 \pm 2(\Delta\alpha)^{1/2})^{1/2}$. The limit of small Γ and $\Delta\alpha$ corresponds physically to the assumption that both the amplifier spacing and the amount of overamplification are small. The stability of these solutions can be determined by letting $\delta = \Gamma^2 \ll 1$ and expanding $U = U_0 + \delta U_1 + \delta^2 U_2 + \cdots$ and $\Delta\alpha = \delta\alpha_1 + \delta^2\alpha_2 + \cdots$. Inserting this into (34) gives

$$U_{0\xi} + \left(-\frac{1}{2}\,\partial_T^2 - U_0^2 + \frac{1}{2}\right)^2 U_0 + \delta[U_{1\xi} + L_- L_+ U_1 - H_1(U_0, \alpha_1)] + \delta^2[U_{2\xi} + L_- L_+ U_2 - H_2(U_0, U_1, \alpha_1, \alpha_2)] + \cdots = 0, \tag{37}$$

where H_n represents the perturbing terms at $O(\delta^n)$ which appear in the equation for U_n, and the operators $L_- = -(1/2)\,\partial_T^2 - U_0^2 + 1/2$ and $L_+ = -(1/2)\,\partial_T^2 - 3\,U_0^2 + 1/2$ are the real and imaginary parts of the linearized NLS [92]. The self-adjoint operators L_+ and L_- are well understood [92].

The dynamics of the solitary wave solutions are exhibited in Figure 26. The stable evolution is demonstrated for the parameter $\gamma = 0.1$. In this case, the upper branch of solutions of the saddle node point $(\eta, \gamma_0) = (1, 0)$ are predicted to be exponentially stable. Indeed, the initial conditions are observed to settle quickly to the final steady-state solution. Below a critical amplitude, however, the solutions decay to zero. The stability region for these solutions was explored in detail elsewhere [93, 94]. For values of $\gamma > 1/4$, the solitary wave solutions destabilize as eigenvalues cross into the right half plane. The dynamics in this case leads to the formation of periodic wave trains which can have complicated structures. These are not considered here since only the pulse solutions are of interest in the context of mode-locking. A more detailed description of the spatial-temporal dynamics of this system which explores a larger class of solutions and their stability is considered by Hewitt and Kutz [95].

Remark: The Figure-Eight Mode-locked Laser. The concept of phase discrimination is certainly not new for mode-locking. In fact, one of the earliest mode-locked lasers, the figure-eight laser, uses phase discrimination to generate a mode-locked pulse train. The concept is much like that of the PSAs, i.e., a pulse with a specific nonlinear phase rotation experiences preferential gain. In the figure-eight laser, this is accomplished via interferometry. Thus specific amplitude pulses are selected since they constructively interfere in the interferometer, whereas pulses which are of higher

or lower amplitude destructively interfere and are preferentially attenuated. This forms the basic workings of the figure-eight laser [5].

5. Beyond Simple Solitons: Break-up, Q-switching, and Interaction. The emphasis in the manuscript thus far has been on models which are capable of producing and stabilizing fundamental solitons. Specifically, the mode-locked pulses are attractors in the laser cavity which can then be used as a source for high-speed fiber-optic communications systems and interconnection networks. In such applications, a uniform pulse train of bits is essential for application purposes. Applications exist, however, where maximal peak powers are required rather than uniform pulse trains. Additionally, laser repetition rates higher than the fundamental cavity round trip time are often required for communication purposes. In both of these cases, the formation of a single mode-locked pulse per round trip with a uniform amplitude is of limited applicability.

Two instabilities in the laser cavity give rise to behavior which is of practical engineering importance. The first instability is known as *Q-switching*. The Q-switching phenomenon is manifested as a slow modulation over the uniform amplitude mode-locked pulse stream. The slow modulation can involve a large number of pulses in the wavetrain, and thus from the perspective of the individual soliton pulses, it is a long-range interaction. The second instability gives rise to the formation of multiple pulses in the laser cavity per round trip. This is easily achieved in the cavity by increasing the pump power of the amplifier. The number of fundamental solitons produced is related to the most energetically favorable configuration [96]. This is often referred to as *harmonic mode-locking*.

Although a variety of other cavity instabilities exists, the two considered here are of practical importance due to increased peak powers (Q-switching) and repetition rates (harmonic mode-locking). In what follows, theoretical models are considered which quantify the observed behavior and underlying mechanisms responsible for these two instabilities. Although the models differ significantly from one another, they are connected by the idea of *pulse-to-pulse interactions*. These interactions, which can be of significantly different time scales and strengths, drive both the Q-switching and harmonic mode-locking behaviors.

5.1. Q-switching. The Q-switching phenomenon has been experimentally observed in both passively and actively mode-locked lasers. Under certain conditions, the intensity of a propagating pulse train develops a modulational structure (or envelope) which varies periodically over a number of pulses. Characterizing the Q-switching as an instability from a uniform wavetrain is difficult using traditional theoretical approaches since they generally consider the dynamics of a single, isolated pulse [11, 12], i.e., a soliton perturbation theory approach. As a consequence, no satisfactory analytical model has been developed to account for both the periodic modulational structure which develops over a pulse train and the parameter regime under which the phenomenon occurs. We consider an active mode-locking model for which Q-switching has been observed [55]. By performing a linear stability analysis of the pulse train solutions, instability is found to be dominated by two unstable growth modes. The two modes have differing propagation constants resulting in beating between the modes. This interaction is sufficient to elucidate the origins of the Q-switching phenomenon. Numerical and analytical evidence confirms the underlying instability mechanism [97].

The physical manifestation of Q-switching can be a beneficial or deleterious effect depending upon the application. Specifically, the pulse train modulation can dra-

matically increase the peak power of portions of the mode-locked pulse train. For spectroscopy [98, 99], multiphoton microscopy [100], and medical applications [101, 102, 103], the increased peak power is advantageous. In contrast, applications in optical communication systems and interconnection networks require a highly uniform power level in the pulse train. Moreover, the higher intensities of the Q-switched pulse train have the potential to exceed the damage threshold of silica-based fiber. Thus the ability to control and manipulate Q-switching is essential for optimizing system performance.

Although typical mode-locking configurations are capable of producing stable and uniform pulse trains, the onset of instabilities such as Q-switching have not been thoroughly understood, aside from an asymptotic analysis of Q-switching as a Hopf bifurcation in a passive mode-locking model [104]. By considering the actively mode-locked laser model (16), the onset of Q-switching can be observed and characterized. The model includes the leading-order physical effects of chromatic dispersion, self-phase modulation, cavity attenuation, bandwidth-limited gain, and an acousto-optic modulator as given by (16). The acousto-optic modulator provides a periodic forcing to the governing equation which allows for preferential gain windows and the onset of mode-locking. The use of the Jacobi elliptic function [56] in (16) allows for the construction of exact pulse train solutions whose behavior can be computed through a linear stability analysis. The Q-switching phenomenon is a result of a beating between the two most unstable eigenmodes which have differing propagation constants. The resulting Q-switched pulse train depends sensitively on the overlap of neighboring pulses. This ultimately determines the Q-switching modulation period and intensity fluctuations. The model provides a characterization of the range of parameters under which stable mode-locking or Q-switching can be expected as a function of the physical specifications of the laser cavity [97].

The exact solution (17) of the governing equation (16) can be analyzed with a standard linear stability analysis. Perturbing around this exact solution, i.e., $Q = k\mathrm{cn}(T,k) + \tilde{Q}\exp(\lambda T)$ with $\tilde{Q} \ll 1$, gives the eigenvalue problem

$$\mathbf{L}\mathbf{v} = \begin{pmatrix} L_1 & L_2 \\ -L_2 + 2k^2\mathrm{cn}^2(T,k) & L_1 \end{pmatrix} \mathbf{v} = \lambda \mathbf{v}, \tag{38}$$

where $\tilde{Q} = R + iI$, $\mathbf{v} = (R \;\; I)^T$, and the self-adjoint operators L_i are given by

$$L_1 = g\tau\frac{\partial^2}{\partial T^2} + g - M\Gamma + M\mathrm{cn}^2(T,k) \quad \text{and} \quad L_2 = -\frac{1}{2}\frac{\partial^2}{\partial T^2} - k^2\mathrm{cn}^2(T,k) + \Omega\,. \tag{39}$$

Note that each operator L_i contains the oscillatory term $\mathrm{cn}^2(T,k)$, which makes it a Hill-type operator [105]. In general, this operator produces a band-gap spectral structure that greatly increases the difficulty of an analytic analysis of (38). Regardless, with a $\mathrm{cn}^2(T,k)$ term, the exact number of band gaps and their location can be found as a function of g, M, and elliptic modulus k. The difficulty, however, is in the matrix structure of the linearized operator $\mathbf{L}$ since it is no longer self-adjoint.

The spectrum of (38) is calculated as a function of the elliptic modulus k. Dependence of the stability on the elliptic modulus has been observed previously [55, 97] and is clearly evident in the operators L_1 and L_2 via the parameters ω, Γ, and M. The eigenmode structure of the two dominant, symmetric and antisymmetric, unstable modes suggests the source of the Q-switching instability. The eigenmode structure of these two specific modes, which are the nodeless ground state and the first excited state, resemble Jacobi elliptic functions of $\mathrm{dn}(T,k)$ and $\mathrm{cn}(T,k)$ type, respectively.

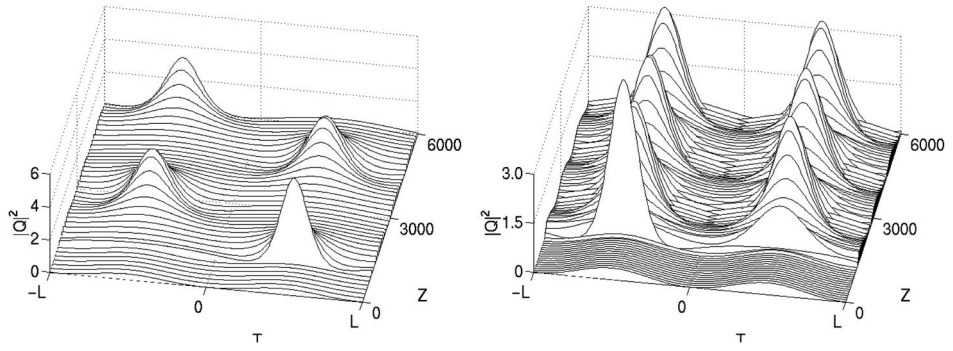

Fig. 27 *Onset of Q-switching starting near the exact solution given by* (17). (a) *One period is considered with the parameters used being* $k = 0.5$, $g = 0.3$, *and* $\tau = 0.1$. (b) *One period is considered with the parameters used being* $k = 0.75$, $g = 0.3$, *and* $\tau = 0.1$.

And since there is a difference in their phase-rotation constants, a beating occurs between these modes which generates the Q-switching phenomenon. In a linear system, the interaction could be easily characterized by superposition. The presence of self-phase modulation in (16) gives a cubic term which does not allow for the application of superposition theory. Regardless, an attempt can be made at characterizing the Q-switching using the superposition principle. Thus a solution of the form [97]

$$Q(Z,T) = A(Z)\mathrm{cn}(T,k) + B(Z)\mathrm{dn}(T,k) \tag{40}$$

is considered where the amplitudes $A = A(Z)$ and $B = B(Z)$ depend upon the propagation distance. Inserting the solution ansatz (40) into (16), assuming $\tau \ll 1$, and applying the rotating wave approximation [87] gives the approximate equations

$$i\frac{dA}{dZ} + \frac{2k^2-1}{2}A + 2(1-k^2)|B|^2A = 0, \tag{41a}$$

$$i\frac{dB}{dZ} + \frac{2-k^2}{2}B + 2(1-1/k^2)|A|^2B = 0, \tag{41b}$$

which can be solved subject to consistency conditions under the rotating-wave approximation to give

$$Q(Z,T) = \frac{1}{\sqrt{3}}\left(k\mathrm{cn}(T,k)\exp\left[i\frac{2k^2-1}{6}Z\right] + \mathrm{dn}(T,k)\exp\left[i\frac{2+k^2}{6}Z\right]\right). \tag{42}$$

Of course, this is only an approximate solution which in no way captures the correct quantitative behavior. However, it does do well in capturing the qualitative behavior observed numerically, i.e., the nonlinear beating between the $\mathrm{cn}(T,k)$ and $\mathrm{dn}(T,k)$ solutions with phase difference $(k^2-3)/6$. The difficulty in making quantitative comparison is due to the marginal validity of the rotating-wave approximation.

The Q-switching dynamics is depicted in Figure 27 for the elliptic modulus values of $k = 0.5$ and $k = 0.75$. Both of these simulations of (16) exhibit the predicted eigenmode interaction approximated by (40) and (42). The quasi-periodic behavior

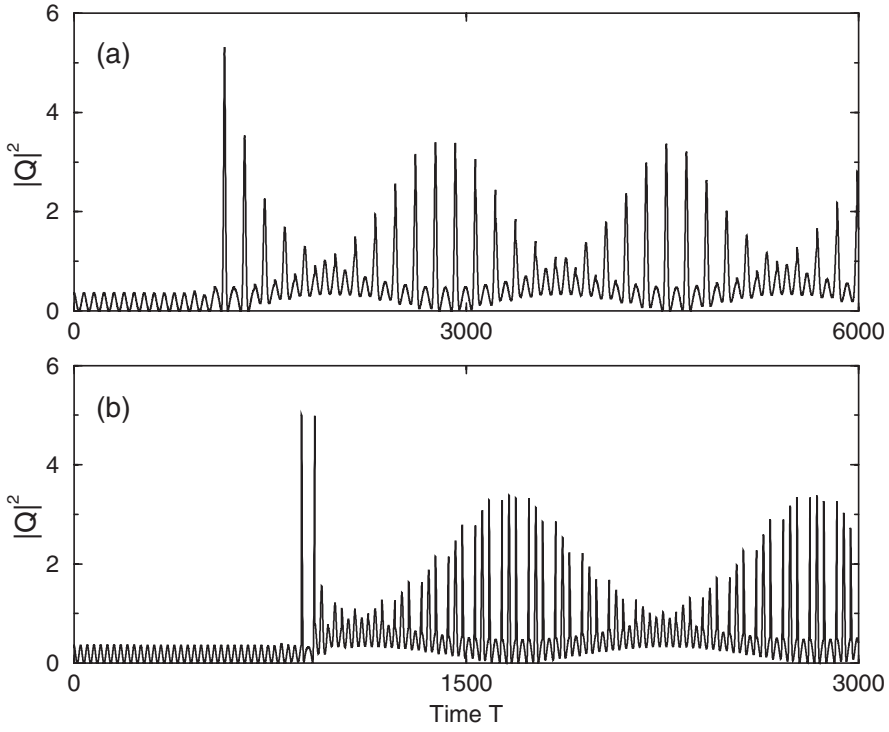

Fig. 28 *Resulting pulse train dynamics for Figure* 27 *in* (a) *and* (b)*, respectively. Note the distinctive Q-switching pattern which results for these unstable runs.*

is clearly k dependent, as is suggested by the linear stability analysis [97]. Thus Q-switching can be understood as a consequence of the quasi-periodic behavior. Specifically, every round trip the quasi-periodic electric field oscillations traverse an output coupler which launches the mode-locked pulses down a optical fiber waveguide. If, for instance, the output coupler is at every $Z = 1$, then the intensity profile $|Q(Z,T)|^2$ is transmitted into the fiber at $Z = n$, where $n = 1, 2, 3, \ldots$. By retrieving these slices of the intensity profile at the various times $Z = n$ and concatenating them, the mode-locked pulse train is constructed. Assuming for convenience that the output coupler is at $Z = n$, then the mode-locked pulse streams for the k values of Figure 27 are given in Figure 28. This shows the dependence of the Q-switching amplitude and frequency on the elliptic modulus k as predicted from the approximate model in the previous subsection. This behavior is the essensce of Q-switching, i.e., a slow modulation of the periodic wavetrain. By controlling the elliptic modulus, the maximum Q-switching power level can be maximized or minimized depending upon the specific engineering application. Qualitatively, this analysis can greatly aid the design of actively mode-locked lasers. For applications which require high peak intensity levels [98, 99, 100, 101, 102, 103], the modulation strength and period should be modified to account for the largest unstable growth modes as a function of the elliptic modulus k, i.e., $k \approx 0.82$ [97]. In contrast, for optical communications, the theory suggests that a strong extinction between well-separated pulses is required in order to avoid the Q-switching instability.

5.2. Harmonic Locking Driven by Gain-Loss Dynamics. Another common phenomenon observed experimentally is harmonic mode-locking [18, 106, 107, 108, 109, 110]. To characterize the harmonic mode-locking, we introduce a time-dependent gain-saturation model. The loss in the laser cavity can be easily incorporated into the NLS (1) by including the intrinsic fiber loss of ≈ 0.20 dB/km and the effective linear losses at the output coupler and mode-locking element. Additionally, it is necessary to include the gain response and its associated relaxation. Once mode-locked, the gain provides a balance with the losses in the laser cavity so that a given intracavity power is preserved. However, the gain-saturation response provides a time-dependent gain across the pulse which is essential in determining the harmonic mode-locking behavior.

We begin by considering only the gain-saturation response without relaxation. This is justified in view of the fact that the ≈ 400 fs mode-locked pulses effectively do not see the relaxation response, which varies from ≈ 4 ms for Cr^{+4}:YAG to ≈ 1 μs for erbium-doped fiber [106]. However, the gain-relaxation between neighboring pulses, which are separated by several microns, will play the key role in the harmonic mode-locking. We can incorporate a gain-saturation behavior into the pulse propagation by considering (1) with a perturbation which simulates the appropriate behavior. Incorporating a time-dependent gain-saturation gives

$$i\frac{\partial Q}{\partial Z} + \frac{1}{2}\frac{\partial^2 Q}{\partial T^2} + |Q|^2 Q - iG\left(1 - 2\frac{\int_{-\infty}^{T} |Q|^2 dT}{\| Q \|^2}\right) Q = 0\,, \tag{43}$$

where G measures the strength of the gain-saturation across the pulse profile and the scalings are as in (12). Note that for $T \to -\infty$ the gain-saturation takes on a constant value of $-G$, while for $T \to \infty$ the gain-saturation is G. Thus, as the pulse traverses the gain medium, the stimulated emission is strongest before the passing of the pulse and then decreases in strength as the inverted gain population is depleted.

The time-dependent gain response gives preferential gain to the part of the pulse which is in front while preferentially attenuating the back of the pulse. This causes the pulse to move to the region of higher gain, i.e., toward $T \to -\infty$. In fact, an analytic, traveling-wave solution exists for (43) which can always be scaled to the form [106]

$$Q = \mathrm{sech}(T - GZ)\exp(iZ/2). \tag{44}$$

This solution suggests that the gain-saturation response is indeed responsible for a drift of the mode-locked pulse to regions of higher gain. Note that the drift velocity is proportional to the gain-saturation response G. We note that the solution (44) is an unstable solution to (43). Thus dispersive radiation which is shed for values of $T - GZ < 0$ will experience a net gain from the time-dependent gain-saturation, which will cause the radiation to grow. However, in practice we must recall that the mode-locking element acts to stabilize the pulse by attenuating low intensity radiation more than the high intensity peak of the pulse [53]. Thus a stabilization is naturally provided in the laser cavity which keeps this gain-saturation destabilization under control.

We consider a periodic laser cavity [106] with a fixed round trip time of T_0 which is illustrated in Figure 29. The separation dynamics can be approximated by

$$\frac{dT_n}{dZ} = \frac{1}{2}(G_n - G_{n+1}), \tag{45}$$

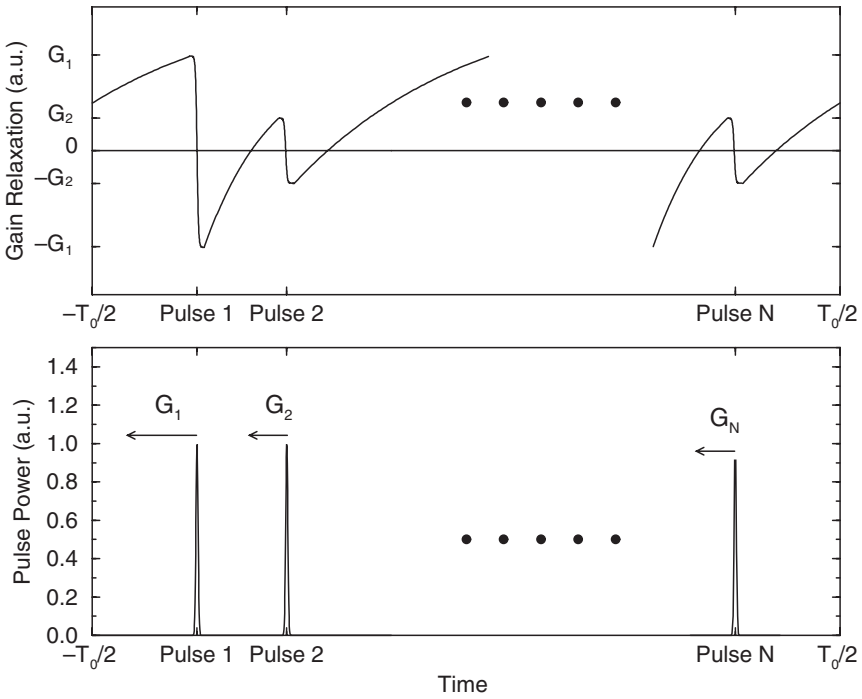

Fig. 29 *Qualitative depiction of the N-pulse interaction dynamics with the gain-saturation behavior. Note the recovery of the gain between pulses and the depletion which occurs across a given pulse.*

where T_n denotes the distance between pulse $n-1$ and pulse n and $T_0 = \sum_{n=1}^{N} T_n$ with $G_{N+1} = G_1$ and $T_{N+1} = T_1$ since the cavity is periodic. An appropriate expression for $G_n - G_{n+1}$ is required in order to determine the interaction dynamics. Following Kutz et al. [106], the interaction is approximated by $\alpha(G_{n+1} - G_n) + G_n = \gamma T_n$, where $\alpha \gg 1$ is a constant of proportionality which depends upon the pulse energy and magnitude of the total gain and $\gamma = T_0/\tau \ll 1$, where τ is the normalized recovery time of the gain medium. Although we cannot solve the system of differential equations (45) explicitly, we can linearize about the steady-state solution for which $G_n = G_{n+1}$. This condition at the critical point implies that

$$T_n = \frac{T_0}{N} \tag{46}$$

is the fixed point since $T_1 + T_2 + \cdots + T_N = T_0$. The stability of this fixed point is found by perturbing about (46) so that $T_n = T_0/N + \tilde{T}_n$. This results in the linearized equations $d\tilde{T}_n/dZ = -(\gamma/2\alpha)\tilde{T}_n$ so that $\tilde{T}_n = \tilde{T}_{n_0} \exp(-\gamma Z/2\alpha)$ and $\tilde{T}_n \to 0$ as $Z \to \infty$. Thus the configuration where T_n is given by (46) is stable, i.e., equally spaced pulses are stable.

The theoretical predictions suggest that the time-dependent gain-relaxation across the pulse causes a pulse drift which effectively acts as a repulsion mechanism for a multiple pulse per round trip laser cavity configuration. The findings are supported by experimental mode-locking results in both fiber and solid-state soliton lasers [106]. Although many alternative physical phenomena may impact harmonic mode-locking performance in other laser cavities, for the low-loss soliton lasers considered here the

gain-relaxation is at least five orders of magnitude larger than the physical mechanisms which include electrostriction, the acoustic effect, soliton-soliton interactions, dispersive radiation-soliton interactions, and the decay time of the SBR structure. The theory requires that the pulses must be spaced closely enough so that the gain is not fully recovered between adjacent pulses. Provided this condition is met, exponentially stable harmonic mode-locking can be achieved. So although this theory does not address the saturation dynamics of the laser or the stability of individual pulses, it does present a model of the pulse-to-pulse interactions which characterize harmonically mode-locked lasers.

5.3. Pulse Bunching Driven by the Acoustic Effect. The harmonic mode-locking considered in the preceding subsection is largely responsible for driving the equally spaced, interpulse interactions in many mode-locked lasers. However, under certain circumstances (e.g., long laser cavities), the gain recovers completely between pulses so that the gain-saturation and gain-depletion play only a limited role in the pulse-to-pulse interactions. In such cavities, other mechanisms play vital roles in determining the eventual pulse spacing. One mechanism which has been proposed to capture the observed pulse bunching in mode-locked lasers operating in the multipulse per round trip regime is the *acoustic effect* [111]. The acoustic effect is driven by an electrostriction mechanism which is induced in the fiber by the high intensities of the mode-locked soliton pulses [112].

From a physical standpoint, the large transverse electric field gradient in single-mode optical fibers creates acoustic waves which act to alter the local index of refraction. Two groups of acoustic modes are of importance: torsional-radial and radial [111]. Only the radial mode is of practical importance since it can appreciably alter the index of refraction. Specifically, each mode-locked pulse sheds an acoustic wave which propagates radially outwards in the fiber. This acoustic wave is reflected back toward the core from the cladding interface and interacts with any mode-locked pulses which are in the core at that time and position. The time scale of the acoustic wave is approximately 1 nanosecond with a 20 nanosecond return time from the cladding. Of course, the cladding attenuates the acoustic wave so that after multiple reflections and several hundred nanoseconds the acoustic wave is lost [111]. During their lifetimes, the acoustic waves generated from the mode-locked pulse stream lead to significant perturbations to the index of refraction.

Index of refraction perturbations in soliton systems lead to *timing jitter* [86]. This can impose a fundamental limit on soliton transmission systems [112]. In a laser cavity, this timing jitter can be responsible for the interpulse spacing dynamics [113]. Characterizing the effects of index perturbations on solitons is easily done in the framework of soliton perturbation theory (see [3] and the references therein). Of interest here is the frequency shift and resulting time shift which occur due to perturbations of the index. In normalized units, the frequency and timing-shift dynamics reduce to a coupled set of differential equations [113]:

$$\frac{d\Omega_j}{dZ} = -\sum_k \frac{d}{dT}\Delta n(T)\bigg|_{T_j - T_k} - \tau\Omega_j, \tag{47a}$$

$$\frac{dT_j}{dZ} = \Omega_j, \tag{47b}$$

where T_j is the center position of the jth pulse, Ω_j is the frequency shift of the jth soliton, and $\Delta n(T)$ is the index perturbation generated by electrostriction [112].

Note that the index perturbation $\Delta n(T)$ is evaluated at each pulse T_k affected by the acoustic wave generated from the jth pulse. The sum over k accounts for the interaction of the jth pulse with the pulses which follow it, and the parameter τ is a restoring force generated by the parabolic gain bandwidth. This interaction can be especially complicated for a short cavity for which the acoustic wave generated by a soliton can self-interact over multiple round trips in the cavity. To perform a simulation, all that remains is to characterize the index response $\Delta n(T)$, which is given in [111].

Simulations of this interaction dynamics show that the acoustic effect generically produces pulse bunching in the laser cavity [113]. This effect, coupled with standard soliton interactions [114] and gain-loss dynamics, can result in a rich and complex pulse interaction dynamics provided the gain dynamics does not dominate and harmonically mode-lock the system [115, 116, 117, 118, 119, 120].

6. Conclusions and Discussion. Considerable interest and research in the past decade have focused on the use of erbium-doped fibers in actively and passively mode-locked fiber lasers operating in both the normal and anomalous dispersion regimes. Many mode-locking schemes have been successfully demonstrated. These include active mode-locking with an acousto-optic modulator, passive mode-locking via nonlinear interferometry in the figure-eight laser, polarization rotation in the ring laser, and a linear cavity configuration which employs a semiconductor structure for fast saturable absorption. A generic feature of each mode-locked laser is the intensity-dependent loss which is achieved by the mode-locking mechanism. The additional loss imparted upon low intensity parts of the pulse, whether it be dispersive radiation or the wings of a pulse, gives the necessary pulse shaping required to achieve stable mode-locking operation. These compact sources of optical pulses near wavelengths of 1.55 microns are key enabling technologies for high-speed fiber-optic communication systems and interconnection networks.

Accurate modeling of these technologically promising mode-locked fiber lasers is essential to their utilization in practical systems. Many models have been developed which attempt to address various aspects of the mode-locking dynamics ranging from the energy equilibration in the cavity to the polarization dynamics of the pulse and the pulse-to-pulse interactions in a harmonic mode-locking configuration. Each model has merit in describing a certain aspect of the laser dynamics, and it is difficult to develop a single model which encompasses all aspects of the mode-locking dynamics. In this paper, we have presented a series of models which address the variety of phenomena driving the mode-locking dynamics. This includes a study of the master mode-locking model which provides the classic qualitative description of the mode-locking process. Extensions of the basic master mode-locking model are also considered which greatly extend the range of parameter space for which stable mode-locked pulse solutions are supported. Quantitative models are then advanced which incorporate more detailed descriptions of the mode-locking mechanisms and allow for direct comparison with experimentally realizable laser cavities.

The qualitative models presented are elegant and universal descriptions of pattern formation models driven beyond equilibrium, i.e., Ginzburg–Landau models. However, it is difficult to make a connection between these qualitative models and realistic mode-locked lasers. On the other hand, the quantitative models are appropriate and realistic descriptions for a wide range of mode-locked laser systems. Further, they help to illustrate that significant progress can be made in understanding the underlying physical mechanisms responsible for mode-locking. Indeed, they help dispel the

common belief in the universal validity of the master mode-locking model. However, the quantitative models lack universal appeal and are often specialized model descriptions. Regardless, they allow for accurate descriptions of physically realizable systems and the range of parameters for which mode-locking can be achieved.

As a final note, the intention in writing this manuscript was to illustrate the wide range of mathematical ideas and models which are required to provide qualitative or quantitative descriptions of mode-locking. Historically, there has been an almost dogmatic adherence to the master mode-locking description due to its universality and overall connection to Ginzburg–Landau-type models (see, for instance, the review article by Haus [4]). However, as demonstrated in the various sections of this manuscript, there is a rich variety of modeling efforts which may be pursued which can provide a much deeper and quantitative understanding of a given mode-locked laser. Many open questions remain concerning the further development of these models and the underlying stability of the generated mode-locked solutions. Given the diverse mathematical background which must be brought to bear on these problems, it is hoped the current manuscript encourages interdisciplinary interactions among mathematicians, physicists, and engineers toward the goal of the continued development and understanding of mode-locked lasers.

Acknowledgments. The author would especially like to thank Keren Bergman, Steve Cundiff, Nail Akhmediev, Brandon Collings, Ben Eggleton, Wayne Knox, and Sergio Tsuda for sharing their practical and experimental expertise in mode-locked lasers. The author is also especially indebted to Karen Intrachat, Todd Kapitula, Arnold Kim, Dave Muraki, Jennifer O'Neil, Joshua Proctor, Bjorn Sandstede, Kristin Spaulding, and Darryl Yong for significant collaborative efforts pertaining to the various models described in this work. Finally, the author acknowledges the tremendous pioneering contributions to the field of mode-locked lasers by the late Hermann A. Haus.

REFERENCES

[1] T. Maiman, *Optical and microwave-optical experiments in ruby*, Phys. Rev. Lett., 4 (1960), pp. 564–566.
[2] A. E. Siegman, *Lasers*, University Science Books, Sausalito, CA, 1986.
[3] H. A. Haus and W. S. Wong, *Solitons in optical communications*, Rev. Modern Phys., 68 (1996), pp. 423–444.
[4] H. A. Haus, *Mode-locking of lasers*, IEEE J. Sel. Top. Quant. Elec., 6 (2000), pp. 1173–1185.
[5] I. N. Duling III and M. L. Dennis, *Compact Sources of Ultrashort Pulses*, Cambridge University Press, Cambridge, UK, 1995.
[6] A. Hasegawa, *Optical Solitons in Fibers*, Springer-Verlag, New York, 1989.
[7] J. K. Shaw, *Mathematical Principles of Optical Fiber Communications*, SIAM, Philadelphia, 2004.
[8] A. Hasegawa and F. Tappert, *Transmission of stationary nonlinear optical pulses in dispersive dielectric fibers*, Appl. Phys. Lett., 23 (1973), pp. 142–170.
[9] M. J. Ablowitz and H. Segur, *Solitons and the Inverse Scattering Transform*, SIAM, Philadelphia, 1981.
[10] N. N. Akhmediev and A. Ankiewics, eds., *Dissipative Solitons*, Lecture Notes in Phys., Springer-Verlag, Berlin, 2005.
[11] H. A. Haus, J. G. Fujimoto, and E. P. Ippen, *Structures for additive pulse mode locking*, J. Opt. Soc. Amer. B Opt. Phys., 8 (1991), pp. 2068–2076.
[12] H. A. Haus, J. G. Fujimoto, and E. P. Ippen, *Analytic theory of additive pulse mode-locking and Kerr lens mode-locking*, IEEE J. Quant. Elec., 28 (1992), pp. 2086–2096.
[13] T. Brabec, C. Spielmann, P. F. Curley, and F. Krausz, *Kerr lens mode locking*, Opt. Lett., 17 (1992), pp. 1292–1294.

[14] L. Spinelli, B. Couilland, N. Goldblatt, and D. K. Negus, *Starting and generation of sub-100 fs pulses in Ti:Al_2 0-2 by self-focusing*, in Conference on Lasers and Electro-Optics, OSA Technical Digest Series, 10 (1991), paper CPDP7.

[15] K. Tamura, H. A. Haus, and E. P. Ippen, *Self-starting additive pulse mode-locked erbium fiber ring laser*, Electron. Lett., 28 (1992), pp. 2226–2228.

[16] H. A. Haus, E. P. Ippen, and K. Tamura, *Additive-pulse mode-locking in fiber lasers*, IEEE J. Quant. Elec., 30 (1994), pp. 200–208.

[17] M. E. Fermann, M. J. Andrejco, Y. Silverberg, and M. L. Stock, *Passive mode-locking by using nonlinear polarization evolution in a polarizing-maintaining erbium-doped fiber laser*, Opt. Lett., 29 (1993), pp. 447–449.

[18] D. Y. Tang, W. S. Man, and H. Y. Tam, *Stimulated soliton pulse formation and its mechanism in a passively mode-locked fibre soliton laser*, Opt. Comm., 165 (1999), pp. 189–194.

[19] I. N. Duling III, *Subpicosecond all-fiber erbium laser*, Electron. Lett., 27 (1991), pp. 544–545.

[20] D. J. Richardson, R. I. Laming, D. N. Payne, V. J. Matsas, and M. W. Phillips, *Self-starting, passively mode-locked erbium fiber laser based on the amplifying Sagnac switch*, Electron. Lett., 27 (1991), pp. 542–544.

[21] M. L. Dennis and I. N. Duling III, *High repetition rate figure eight laser with extracavity feedback*, Electron. Lett., 28 (1992), pp. 1894–1896.

[22] F. Ö. Ilday, F. W. Wise, and T. Sosnowski, *High-energy femtosecond stretched-pulse fiber laser with a nonlinear optical loop mirror*, Opt. Lett., 27 (2002), pp. 1531–1533.

[23] F. X. Kärtner and U. Keller, *Stabilization of solitonlike pulses with a slow saturable absorber*, Opt. Lett., 20 (1995), pp. 16–18.

[24] B. Collings, S. Tsuda, S. Cundiff, J. N. Kutz, M. Koch, W. Knox, and K. Bergman, *Short cavity Erbium/Ytterbium fiber lasers mode-locked with a saturable Bragg reflector*, IEEE J. Selec. Top. Quant. Elec., 3 (1997), pp. 1065–1075.

[25] S. Tsuda, W. H. Knox, E. A. DeSouza, W. J. Jan, and J. E. Cunningham, *Low-loss intracavity AlAs/AlGaAs saturable Bragg reflector for femtosecond mode-locking in solid-state lasers*, Opt. Lett., 20 (1995), pp. 1406–1408.

[26] F. X. Kärtner, D. Kopf, and U. Keller, *Solitary pulse stabilization and shortening in actively mode-locked lasers*, J. Opt. Soc. Amer. B Opt. Phys., 12 (1994), pp. 486–496.

[27] H. A. Haus, *A theory of forced mode locking*, IEEE J. Quant. Elec., 11 (1975), pp. 323–330.

[28] J. N. Kutz, *Mode-locking of fiber lasers via nonlinear mode-coupling*, in Dissipative Solitons, Lecture Notes in Phys., N. N. Akhmediev and A. Ankiewics, eds., Springer-Verlag, Berlin, 2005, pp. 241–265.

[29] A. Gordon and B. Fischer, *Phase transition theory of many-mode ordering and pulse formation in lasers*, Phys. Rev. Lett., 89 (2002), article 103901.

[30] A. Gordon and B. Fischer, *Phase transition theory of pulse formation in passively mode-locked lasers with dispersion and Kerr nonlinearity*, Opt. Comm., 223 (2003), pp. 151–156.

[31] A. Gordon and B. Fischer, *Statistical mechanics theory for active mode locking with noise*, Opt. Lett., 29 (2004), pp. 1022–1024.

[32] I. P. Christov, V. Stoev, M. Murname, and H. Kapteyn, *Sub-10 fs operation of Kerr-lens mode-locked lasers*, Opt. Lett., 21 (1996), pp. 1493–1495.

[33] I. P. Christov, M. M. Murname, H. C. Kapteyn, J. P. Zhou, and C. P. Huang, *Fourth-order dispersion limited solitary pulses*, Opt. Lett., 19 (1994), pp. 1465–1466.

[34] N. R. Pereira and L. Stenflo, *Nonlinear Schrödinger equation including growth and damping*, Phys. Fluids, 20 (1977), pp. 1733–1734.

[35] C.-J. Chen, P. K. A. Wai, and C. R. Menyuk, *Soliton fiber ring laser*, Opt. Lett., 17 (1992), pp. 417–419.

[36] T. Kapitula, J. N. Kutz, and B. Sandstede, *Stability of pulses in the master mode-locking equation*, J. Opt. Soc. Amer. B Opt. Phys., 19 (2002), pp. 740–746.

[37] T. Kapitula, J. N. Kutz, and B. Sandstede, *The Evans function for nonlocal equations*, Indiana J. Math., 53 (2004), pp. 1095–1126.

[38] T. Kapitula, *Stability criterion for bright solitary waves of the perturbed cubic-quintic Schrödinger equation*. Phys. D, 116 (1998), pp. 95–120.

[39] M. Romagnoli, S. Wabnitz, P. Franco, M. Midrio, L. Bossalini, and F. Fontana, *Role of dispersion in pulse emission from a sliding-frequency fiber laser*, J. Opt. Soc. Amer. B Opt. Phys., 12 (1995), pp. 938–944.

[40] M. Romagnoli, S. Wabnitz, P. Franco, M. Midrio, F. Fontana, and G. E. Town, *Tunable erbium-ytterbium fiber sliding-frequency soliton laser*, J. Opt. Soc. Amer. B Opt. Phys., 12 (1995), pp. 72–76.

[41] N. Akhmediev, J. M. Soto-Crespo, and G. Town, *Pulsating solitons, chaotic solitons, period doubling, and pulse coexistence in mode-locking lasers: Complex Ginzburg–Landau equation approach*, Phys. Rev. E, 63 (2001), article 056602.

[42] J. M. Soto-Crespo and N. Akhmediev, *Composite solitons and two-pulse generation in passively mode-locked lasers modeled by the complex quintic Swift-Hohenberg equation*, Phys. Rev. E, 66 (2002), article 066610.
[43] J. M. Soto-Crespo, N. Akhmediev, K. S. Chiang, *Simultaneous existence of multiplicity of stable and unstable solitons in dissipative systems*, Phys. Lett. A, 291 (2001), pp. 115–123
[44] F. X. Kärtner, D. Kopf, and U. Keller, *Solitary pulse stabilization and shortening in actively mode-locked lasers*, J. Opt. Soc. Amer. B Opt. Phys., 12 (1995), pp. 486–496.
[45] M. Cross and P. Hohenberg, *Pattern formation outside of equilibrium*, Rev. Modern Phys., 65 (1993), pp. 851–1112.
[46] S. T. Cundiff, J. M. Soto-Crespo, and N. Akhmediev, *Experimental evidence for soliton explosions*, Phys. Rev. Lett., 88 (2002), article 073903.
[47] A. Hasegawa and Y. Kodama, *Guiding-center soliton in fibers with periodically varying dispersion*, Opt. Lett., 16 (1991), pp. 1385–1387.
[48] J. C. Bronski and J. N. Kutz, *Guiding-center pulse dynamics in nonreturn-to-zero (return-to-zero) communications system with mean-zero dispersion*, J. Opt. Soc. Amer. B Opt. Phys., 14 (1997), pp. 903–911.
[49] H. Haug and S. W. Koch, *Quantum Theory of the Optical and Electronic Properties of Semiconductors*, 3rd ed., World Scientific, Singapore, 1994, pp. 317–327.
[50] D. S. Chemla, W. H. Knox, D. A. B. Miller, S. Schmitt-Rink, J. B. Stark, and R. Zimmermann, *The excitonic optical Stark effect in semiconductor quantum wells probed with femtosecond optical pulses*, J. Luminescence, 44 (1989), pp. 233–246.
[51] W. H. Knox, D. S. Chemla, D. A. B. Miller, J. B. Stark, and S. Schmitt-Rink, *Femtosecond ac Stark effect in semiconductor quantum wells: Extreme low- and high-intensity limits*, Phys. Rev. Lett., 62 (1989), pp. 1189–1192.
[52] D. A. B. Miller, *Quantum well optical switching devices*, in Confined Electrons and Photons, E. Burnstein and C. Weisbuch, eds., Plenum, New York, 1995, pp. 675–701.
[53] J. N. Kutz, B. C. Collings, K. Bergman, S. Tsuda, S. Cundiff, W. H. Knox, P. Holmes, and M. Weinstein, *Mode-locking pulse dynamics in a fiber laser with a saturable Bragg reflector*, J. Opt. Soc. Amer. B Opt. Phys., 14 (1997), pp. 2681–2690.
[54] E. Zauderer, *Partial Differential Equations of Applied Mathematics*, 2nd ed., John Wiley, New York, 1989, pp. 426–446.
[55] J. J. O'Neil, J. N. Kutz, and B. Sandstede, *Analytic theory for actively mode-locked fiber lasers*, IEEE J. Quant. Elec., 38 (2002), pp. 1412–1419.
[56] M. Abramowitz and I. A. Stegun, *Handbook of Mathematical Functions*, National Bureau of Standards, Washington, D.C., 1964.
[57] S. V. Manakov, *On the theory of two-dimensional stationary self-focusing of electro-magnetic waves*, Soviet Phys. JETP, 38 (1974), pp. 248–253.
[58] S. Trillo, S. Wabnitz, E. M. Wright, and G. I. Stegeman, *Polarized soliton instability and branching in birefringent fibers*, Opt. Comm., 70 (1989), pp. 166–172.
[59] D. J. Muraki and W. L. Kath, *Hamiltonian dynamics of solitons in optical fibers*, Phys. D, 48 (1991), pp. 53–64.
[60] C. R. Menyuk, *Pulse propagation in an elliptically birefringent Kerr media*, IEEE J. Quant. Elec., 25 (1989), pp. 2674–2682.
[61] C. R. Menyuk, *Nonlinear pulse propagation in birefringent optical fibers*, IEEE J. Quant. Elec., 23 (1987), pp. 174–176.
[62] A. D. Kim, J. N. Kutz, and D. Muraki, *Pulse-train uniformity in optical fiber lasers passively mode-locked by nonlinear polarization rotation*, IEEE J. Quant. Elec., 36 (2000), pp. 465–471.
[63] K. Spaulding, D. H. Yong, A. D. Kim, and J. N. Kutz, *Nonlinear dynamics of mode-locking optical fiber ring lasers*, J. Opt. Soc. Amer. B Opt. Phys., 19 (2002), pp. 1045–1054.
[64] D. Y. Tang, W. S. Man, H. Y. Tam, and M. S. Demokan, *Modulational instability in a fiber soliton ring laser induced by periodic dispersion variation*, Phys. Rev. A, 61 (2000), article 023804.
[65] W. S. Man, H. Y. Tam, M. S. Demokan, P. K. A. Wai, and D. Y. Tang, *Mechanism of intrinsic wavelength tuning and sideband asymmetry in a passively mode-locked soliton fiber ring laser*, J. Opt. Soc. Amer. B Opt. Phys., 17 (2000), pp. 28–33.
[66] B. C. Collings, S. T. Cundiff, N. N. Akhmediev, J. M. Soto-Crespo, K. Bergman, and W. H. Knox, *Polarization locked temporal vector solitons in a fiber laser: Experiment*, J. Opt. Soc. Amer. B Opt. Phys., 17 (2000), pp. 354–365.
[67] S. T. Cundiff, B. C. Collings, N. Akhmediev, J. M. Soto-Crespo, K. Bergman, and W. H. Knox, *Observation of polarization-locked vector solitons in optical fiber*, Phys. Rev. Lett., 82 (1999), pp. 3988–3991.

[68] A. M. Vengsarkar, P. J. Lemaire, J. B. Judkins, V. Bhatia, T. Erdogan, and J. E. Sipe, *Long-period fiber gratings as band-rejection filters*, J. Light. Tech., 14 (1996), pp. 58–65.
[69] B. J. Eggleton, R. E. Slusher, J. B. Judkins, J. B. Stark, and A. M. Vengsarkar, *All-optical switching in long-period fiber gratings*, Opt. Lett., 22 (1997), pp. 883–885.
[70] S. M. Jensen, *The nonlinear coherent coupler*, IEEE J. Quant. Elec., 18 (1982), pp. 1580–1583.
[71] H. G. Winful and D. T. Walton, *Passive mode locking through nonlinear coupling in a dual-core fiber laser*, Opt. Lett., 17 (1992), pp. 1688–1690.
[72] Y. Oh, S. L. Doty, J. W. Haus, and R. L. Fork, *Robust operation of a dual-core fiber ring laser*, J. Opt. Soc. Amer. B Opt. Phys., 12 (1995), pp. 2502–2507.
[73] D. Marcuse, *Theory of Dielectric Optical Waveguides*, Academic, New York, 1974.
[74] J. N. Kutz, B. J. Eggleton, J. B. Stark, and R. E. Slusher, *Nonlinear pulse propagation in long-period fiber gratings: Theory and experiment*, IEEE J. Selec. Top. Quant. Elec., 3 (1997), pp. 1232–1245.
[75] K. Intrachat and J. N. Kutz, *Theory and simulation of passive mode-locking dynamics using a long period fiber grating*, IEEE J. Quant. Elec., 39 (2003), pp. 1572–1578.
[76] D. N. Christodoulides and R. I. Joseph, *Discrete self-focusing in nonlinear arrays of coupled waveguides*, Opt. Lett., 13 (1988), pp. 794–796.
[77] H. S. Eisenberg, Y. Silberberg, R. Morandotti, A. R. Boyd, and J. S. Aitchison, *Discrete spatial optical solitons in waveguide arrays*, Phys. Rev. Lett., 81 (1998), pp. 3383–3386.
[78] A. B. Aceves, C. De Angelis, T. Peschel, R. Muschall, F. Lederer, S. Trillo, and S. Wabnitz, *Discrete self-trapping, soliton interactions, and beam steering in nonlinear waveguide arrays*, Phys. Rev. E, 53 (1996), pp. 1172–1189.
[79] H. S. Eisenberg, R. Morandotti, Y. Silberberg, J. M. Arnold, G. Pennelli, and J. S. Aitchison, *Optical discrete solitons in waveguide arrays.* I. *Soliton formation*, J. Opt. Soc. Amer. B Opt. Phys., 19 (2002), pp. 2938–2944.
[80] U. Peschel, R. Morandotti, J. M. Arnold, J. S. Aitchison, H. S. Eisenberg, Y. Silberberg, T. Pertsch, and F. Lederer, *Optical discrete solitons in waveguide arrays.* II. *Dynamic properties*, J. Opt. Soc. Amer. B Opt. Phys., 19 (2002), pp. 2637–2644.
[81] J. Proctor and J. N. Kutz, *Passive mode-locking using waveguide arrays*, Opt. Lett., 30 (2005), pp. 2013–2015.
[82] T. Pertsch, U. Peschel, J. Kobelke, K. Schuster, H. Bartelt, S. Nolte, A. Tünnermann, and F. Lederer, *Nonlinearity and disorder in fiber arrays*, Phys. Rev. Lett., 93 (2004), article 053901.
[83] M. Asobe, T. Kanamori, and K. Kubodera, *Applications of highly nonlinear chalcogenide glass fibers in ultrafast all-optical switches*, IEEE J. Quant. Elec., 29 (1993), pp. 2325–2333.
[84] M. Asobe, T. Ohara, I. Yokohoma, and T. Kaino, *Fabrication of Bragg grating in chalcogenide glass fiber using transverse holographic method*, Electron. Lett., 32 (1996), pp. 1611–1613.
[85] H. Yuen, *Reduction of quantum fluctuation and suppression of the Gordon-Haus effect with phase-sensitive linear amplifiers*, Opt. Lett., 17 (1992), pp. 73–75.
[86] J. P. Gordon and H. A. Haus, *Random walk of coherently amplified solitons in optical fiber transmission,* Opt. Lett., 11 (1986) pp. 665–667.
[87] R. W. Boyd, *Nonlinear Optics*, Academic Press, New York, 1992.
[88] J. N. Kutz, W. L. Kath, R.-D. Li, and P. Kumar, *Long-distance pulse propagation in nonlinear optical fibers using periodically-spaced parametric amplifiers*, Opt. Lett., 18 (1993), pp. 802–804.
[89] J. N. Kutz, C. V. Hile, W. L. Kath, R.-D. Li, and P. Kumar, *Pulse propagation in nonlinear optical fiber-lines that employ phase-sensitive parametric amplifiers*, J. Opt. Soc. Amer. B Opt. Phys., 11 (1994), pp. 2112–2123.
[90] C. M. Bender and S. A. Orszag, *Advanced Mathematical Methods for Scientists and Engineers*, McGraw-Hill, New York, 1978.
[91] J. Kevorkian and J. D. Cole, *Perturbation Methods in Applied Mathematics*, Springer-Verlag, New York, 1981.
[92] M. I. Weinstein, *Modulational stability of ground states of nonlinear Schrödinger equations*, SIAM J. Math. Anal., 16 (1985), pp. 472–491.
[93] J. N. Kutz and W. L. Kath, *Stability of pulses in nonlinear optical fibers using phase-sensitive amplifiers*, SIAM J. Appl. Math., 56 (1996), pp. 611–626.
[94] J. C. Alexander, M. G. Grillakis, C. K. R. T. Jones, and B. Sandstede, *Stability of pulses on optical fibers with phase-sensitive amplifiers*, Z. Angew. Math. Phys., 48, (1997), pp. 175–192.
[95] S. E. Hewitt and J. N. Kutz, *Dynamics of the optical parametric oscillator near resonance detuning*, SIAM J. Appl. Dyn. Syst., 4 (2005), pp. 808–831.

[96] S. Namiki, E. P. Ippen, H. Haus, and C. X. Yu, *Energy equations for mode-locked lasers*, J. Opt. Soc. Amer. B Opt. Phys., 14 (1997), pp. 2099–2111.
[97] J. Proctor and J. N. Kutz, *Theory of Q-switching in actively mode-locked lasers*, J. Opt. Soc. Amer. B Opt. Phys., 23 (2006), pp. 652–662.
[98] G. L. Eesley, *Generation of nonequilibrium electron and lattice temperature in copper by picosecond laser pulses*, Phys. Rev. B, 33 (1986), pp. 2144–2151.
[99] V. I. Klimov and D. W. McBranch, *Femtosecond high-sensitivity, chirp-free transient absorption spectroscopy using kilohertz lasers*, Opt. Lett., 23 (1998), pp. 277–279.
[100] J. A. Squier, M. Müller, G. J. Brakenhoff, and K. R. Wilson, *Third harmonic generation microscopy*, Opt. Expr., 3 (1998), pp. 315–324.
[101] J. -M. Hopkins and W. Sibbett, *Big payoffs in a flash*, Sci. Amer., (2000), pp. 73–79.
[102] G. A. Mourou and D. Umdstader, *Extreme light*, Sci. Amer., (September 2002), pp. 63–68.
[103] L. da Silva, M. Perry, M. Feit, and B. Stuart, *The short-pulse laser: a safe, painless surgical tool*, Science & Tech. Rev., (October 1995), pp. 29–31.
[104] T. Kolokolnikov, M. Nizette, T. Erneux, N. Joly, and S. Bielawski, *The Q-switching instability in passively mode-locked lasers*, Phys. D, 219 (2006), pp. 13–21.
[105] W. Magnus, *Hill's Equation*, Wiley, New York, 1966.
[106] J. N. Kutz, B. C. Collings, K. Bergman, and W. H. Knox, *Stabilized pulse spacing in soliton lasers due to gain depletion and recovery*, IEEE J. Quant. Elec., 34 (1998), pp. 1749–1757.
[107] B. Collings, K. Berman, and W. H. Knox, *Stable multigigahertz pulse train formation in a short cavity passively harmonic modelocked Er/Yb fiber laser*, Opt. Lett., 23 (1998), pp. 123–125.
[108] M. E. Fermann and J. D. Minelly, *Cladding-pumped passive harmonically mode-locked fiber laser*, Opt. Lett., 21 (1996), pp. 970–972.
[109] A. B. Grudinin, D. J. Richardson, and D. N. Payne, *Energy quantization in figure eight fibre laser*, Electron. Lett., 28 (1992), pp. 1391–1393.
[110] M. J. Guy, P. U. Noske, A. Boskovic, and J. R. Taylor, *Femtosecond soliton generation in a praseodymium fluoride fiber laser*, Opt. Lett., 19 (1994), pp. 828–830.
[111] E. M. Dianov, A. V. Luchnikov, A. N. Pilipetskii, and A. N. Starodumov, *Electrostriction mechanism of soliton interaction in optical fibers*, Opt. Lett., 15 (1990), pp. 314–316.
[112] E. M. Dianov, A. V. Luchnikov, A. N. Pilipetskii, and A. M. Prokhorov, *Longrange interaction of picosecond solitons through excitation of acoustic waves in optical fibers*, Appl. Phys. B, 54 (1992), pp. 175–180.
[113] A. N. Pilipetskii, E. A. Golovchenck, and C. R. Menyuk, *Acoustic effect in passively mode-locked fiber ring lasers*, Opt. Lett., 20 (1995), pp. 907–909.
[114] J. P. Gordon, *Interaction forces among solitons in optical fibers*, Opt. Lett., 8 (1983), pp. 396–398.
[115] R. P. Davey, N. Langford, and A. I. Ferguson, *Interacting solutions in erbium fibre laser*, Electron. Lett., 27 (1991), pp. 1257–1259.
[116] M. J. Lederer, B. Luther-Davis, H. H. Tan, C. Jagadish, N. N. Akhmediev, and J. M. Soto-Crespo, *Multipulse operation of a Ti:Sapphire laser mode locked by an ion-implanted semiconductor saturable-absorber mirror*, J. Opt. Soc. Amer. B Opt. Phys., 16 (1999), pp. 895–904.
[117] Q. Xing, L. Chai, W. Zhang, and Ch.-yue Wang, *Regular, period-doubling, quasi-periodic, and chaotic behavior in a self-mode-locked Ti:sapphire laser*, Opt. Comm., 162 (1999), pp. 71–74.
[118] M. Lai, J. Nicholson, and W. Rudolph, *Multiple pulse operation of a femtosecond Ti:sapphire laser*, Opt. Comm., 142 (1997), pp. 45–49.
[119] Ch.-Y. Wang, W. Zhang, K. F. Lee, and K. M. Yoo, *Pulse splitting in a self-mode-locking Ti:sapphire laser*, Opt. Comm., 137 (1997), pp. 89–92.
[120] H. Kitano and S. Kinoshita, *Stable multipulse generation from a self-mode-locked Ti:sapphire laser*, Opt. Comm., 157 (1998), pp. 128–134.